Heat Flux Measurements from a Human Forearm under Natural Convection and Isothermal Jets

Shyam Krishna Shenoy Ajith N P Shenoy

Thesis submitted to the faculty of the Virginia Polytechnic Institute and State University in partial fulfillment of the requirements for the degree of

Master of Science

In

Mechanical Engineering

Thomas E. Diller, Chair

Scott T. Huxtable

Alfred L. Wicks

July 27, 2017

Blacksburg, Virginia

Keywords: Thermal comfort, Frossling number, Isothermal jets, Jet impingement, Thermal Microenvironment, Heat transfer

Heat Flux Measurements from a Human Forearm under Natural Convection and Isothermal Jets

Shyam Krishna Shenoy Ajith N P Shenoy

Abstract

This work is an experimental study on heat transfer from a human arm and a model cylinder. Heat transfer from a human forearm to a large jet, representative of a building HVAC vent/outlet was studied using both an IR camera and a heat flux sensor. The isothermal jet was discharged horizontally from a wind tunnel, at the same temperature as the ambient air.

The model cylinder was used to validate the heat transfer results with results from previous studies, using both the IR camera and heat flux sensors. Further, a study on heat transfer to impingement jets from a human forearm at various Reynolds numbers (Re = 9500-41000) and impinging distances of four and eight jet diameters was done. Heat transfer from a human arm to such impingement jets were then compared with heat transfer due to natural convection under both open and controlled environments. A significant increase in convection heat transfer with Reynolds number and distance from the jet outlet was observed. A nearly four-fold increase in convection heat transfer coefficient was obtained when a jet with Reynolds number of 9500 was impinged on a human arm when compared to that obtained under natural convection in an open environment. Empirical correlations for predicting the stagnation and average Nusselt number from a human arm were also developed with high values of correlation coefficients for future studies. Impingement jets were found to be an effective means to transfer heat from human bodies and could potentially be used for creating thermally conditioned microenvironments.

Heat Flux Measurements from a Human Forearm under Natural Convection and Isothermal Jets

Shyam Krishna Shenoy Ajith N P Shenoy

General Audience Abstract

Impingement jets have been used in a variety of applications such as turbine cooling, electronic cooling and for annealing of metals for enhancing heat transfer due to its large convective heat transfer rates. This study aims at studying the heat transfer to such jets from a human arm and a model cylinder and its potential use in creating thermally conditioned microenvironments in buildings. Thermal microenvironment conditioning refers to controlling the thermal properties of a small zone around the individuals to be conditioned, based on the thermal behavior of the individual. This reduces overall energy consumption by restricting air conditioning to a small area around individuals and can also be potentially be used to cater to the individual occupant's thermal comfort. Therefore, a large jet representative of an HVAC outlet in buildings was used for this purpose. A horizontal, isothermal jet of air was impinged on a human forearm over a range of jet velocities and the resulting heat transfer rates were compared to that obtained under natural convection (in an open as well as a controlled setting). An IR camera and heat flux sensors were used to measure the heat transfer rates. A nearly four-fold increase in convection heat transfer coefficient was obtained when a jet with Reynolds number of 9500 was impinged on a human arm when compared to that obtained under natural convection in an open environment. Empirical correlations were developed to predict heat transfer from the jet at a given jet velocity with high values of correlation coefficients. Overall, impingement jets were found to be an effective means to transfer heat from human bodies and could potentially be used for creating thermally conditioned microenvironments.

"Without data, you're just another person with an opinion." — W. Edwards Deming

Dedication

This dissertation is dedicated to my family for their endless love and support throughout my journey. Without your encouragement and motivation, this work would not have been possible.

Acknowledgements

I am grateful to everyone who has helped and guided me in various ways and forms throughout my Masters career. I would first like to thank my advisor, Dr. Diller for providing me the opportunity to be a part of his research group and for giving time, effort and knowledge to aid in the completion of this work. Your guidance and experience has taken me closer to being a complete well-rounded engineer. I would also like to thank Dr. Huxtable and Dr. Wicks for their support and willingness to be a part of my thesis committee.

Next, I would like to acknowledge Karthik for helping me understand his work, the work that was done before in this field and for providing me a solid foundation of knowledge and support. I also want to thank Abdul, Ali, Chris and Rande for being such awesome lab mates and for making work in the lab a fun activity. They provided me friendship and a lot of support while working in the lab. I wish them good luck in their endeavors.

Last but not the least; I would like to thank my family and friends for their unwavering support and encouragement.

Table of Contents

List of Figures

List of Tables

Nomenclature

A	Surface area of the heater (m^2)
D	Diameter of the cylinder (m)
d	Diameter of the jet nozzle (m)
h	Heat transfer coefficient (W/m^2-K)
H.F.	Heat Flux
IR	Infrared
k	Thermal conductivity (W/m-K)
N.C.	Natural convection
q"	Heat flux (W/m^2)
R	Resistance (Ω)
S	sensitivity of the heat flux sensor ($V/W/m^2$)
T	Temperature (^0C)
t	thickness
v	Centerline jet velocity (m/s)
V	Voltage (V)
z	Impinging distance from the jet origin (m)
θ	Angle with respect to the impingement point or horizontal (degrees)
ε	Emissivity of the surface
σ	Stefan-Boltzmann constant

Non-dimensional Numbers

Fr	Frossling number; $\left(\frac{Nu}{\sqrt{Re_D}}\right)$
Nu	Local Nusselt number; $\left(\frac{hD}{k}\right)$
Re_D	Reynolds number based on cylinder diameter; $\left(\frac{\rho U_0 D}{\mu}\right)$

Subscripts

0	Jet exit properties
Al	Aluminum
avg	Average
cond	conduction
conv	convection
in	input properties of the heater
inf	Ambient fluid properties
r	radial direction
rad	radiation
s	Distance along the circumference of the cylinder (m)

1. Chapter Organization

This dissertation has been organized into six chapters. Chapter 2 introduces the fundamentals characteristics of isothermal impingement jet flow, how such jets aide in increasing heat transfer and previous studies that helped in understanding the major factors affecting the heat transfer from a cylinder to such an impingement jet. It also includes a brief introduction to heat transfer from a human body, parameters governing the heat transfer and previous studies on heat transfer from human body to various types of jets.

Chapter 3 discusses in detail the experimental setup for carrying out isothermal jet impingement studies and natural convection studies on a heated cylinder and a human forearm. It also details the construction of the cylinder and details regarding placement of IR camera to avoid errors in temperature measurement due to directional emissivity from a curved surface.

Chapter 4 describes how the temperature and heat flux data measured during the experiments was used to extract various parameters and non-dimensional quantities, and the calculation of their uncertainty.

Chapter 5 discusses the experimental results obtained from the jet impingement and natural convection studies and how heat transfer varies under these conditions.

Chapter 6 summarizes the main outcomes of the experiments and the subsequent data reduction analysis. It also identifies possible future work that could be done based on this study and contains recommendations that would help broaden the scope of this research.

Six appendices have also been included in this thesis. Appendix A explains the method used for calculating uncertainties of various parameters along with specific examples. Appendix B shows the procedure and results obtained for estimation of convection heat transfer coefficient of a human forearm based on previous results. Appendix C shows the procedure for construction of a paper grid for measurement of angles using an IR camera. Appendix D explains the methodology and results of quantification of the range of IR camera viewing angle for accounting the directional emissivity of curved surfaces. Appendix E details the construction of the control environment used for conducting natural convection experiments. Appendix F

shows the plots of individual experiments for heat transfer from natural convection from a human forearm and a heated cylinder in both open and controlled environments

2. Introduction

Microenvironment conditioning refers to controlling the thermal properties of a small zone around the object to be conditioned, based on the thermal behavior of the object [1]. Such a system can be used to cater to the comfort needs of multiple individuals and at the same time, reduce energy consumption needs for air conditioning of building spaces. Microenvironment creation units currently available in the market are either floor mounted or desk mounted [2]. For a working model of a system as proposed in this study, the traditional HVAC vent system was replaced with a nozzle with directional flexibility, so that the jet can be maneuvered to aim the flow of air at a different direction as needed. The present study aims to measure the heat transfer characteristics of a horizontal isothermal jet of diameter, d, impinging on a human arm in such a thermal microenvironment, over a range of Reynolds numbers. A cylinder of diameter 'D', similar to the diameter of a human arm, was used to validate heat transfer results using an IR camera and heat flux sensors with results from previous studies. Experiments on the circumferential variation of heat transfer to impingement jets from a human forearm were performed and was measured using a heat flux sensor and was compared with the heat transfer results obtained using natural convection.

2.1. Introduction to Isothermal jets

A submerged isothermal jet is a discharge of fluid into another fluid, which is at the same temperature as the jet fluid. In addition, a jet is called a free jet if it does not interact with any medium other than its surrounding. Several studies have been done on the variation of centerline velocities of free jets and the phenomena that surround it. An isothermal jet exiting a nozzle has three regions depending on the relative distance from the nozzle, namely, the initial region or potential region, the transition region and the fully developed region as shown in figure 1 [3]. In the initial region, which is the closest to the nozzle, the jet begins interacting with the surrounding stationary fluid and a shear layer develops because of the viscous effects of the static surrounding fluid. This mixing causes momentum transfer between the jet and the ambient air and causes the jet to slow down and widen its shape. However, this effect of slowing down does

not affect the velocity of the centerline of the jet until a certain distance. The region until this distance is called the potential/initial region and the distance is called the potential core length.

Beyond the potential core region, the centerline velocity continues to decrease and the overall velocity profile of the jet continues to vary through the transitional region. At the end of the transitional region, the jet takes the shape of a Gaussian distribution and continues to be so for all further distances [4]. This region, which starts at the end of the transitional region, is called the main region of the jet. The rate of decrease of centerline velocity in the main region was found to be inversely proportional to the distance from the exit.

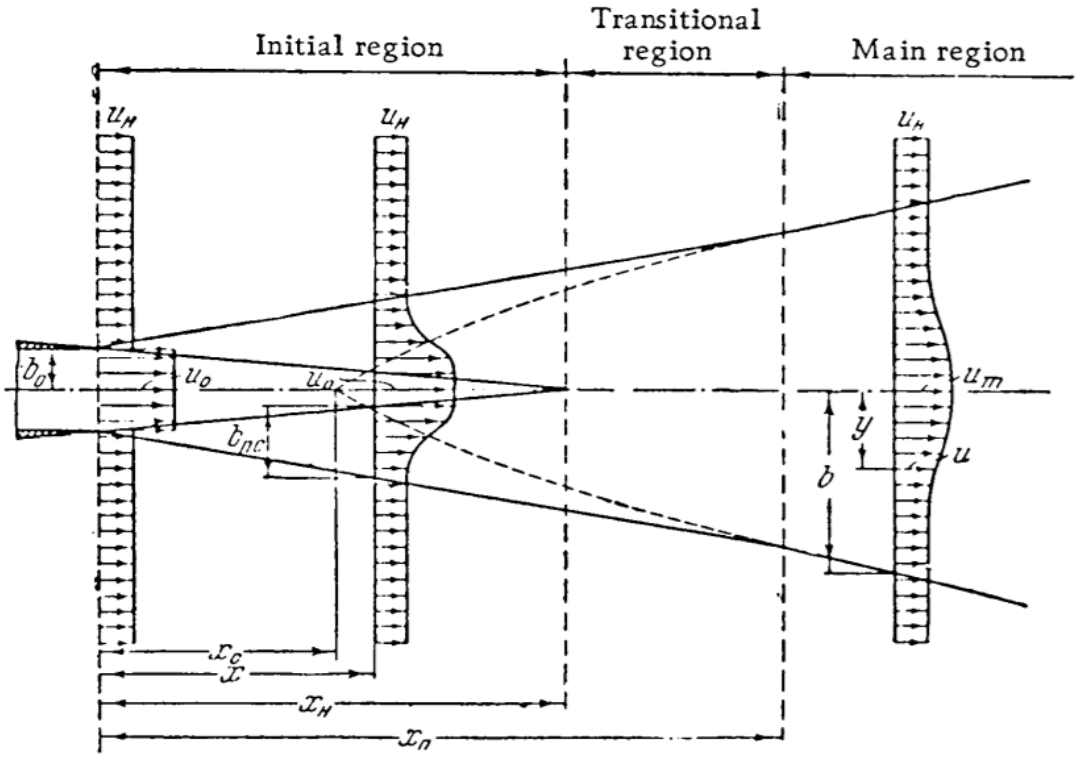

Figure 1: Regions of A free Jet, Abramovich G.N, Schindel L., The Theory of Turbulent Jets, MIT press, 2003, used under fair use,2016

2.2. Background on heat transfer using impingement jets

Impingement jets have been used in a variety of applications to provide high convective heat transfer rates, including cooling of stock material during material forming processes [5], cooling of electronic components

and turbine components, and other industrial processes. A range of uses and performance of impingement jets can be found in a number of reviews [4][6][7]. Heat transfer from an isothermal impingement jet of air depends on the curvature of the cylinder relative to the jet nozzle diameter, the distance of the cylinder from the jet nozzle relative to the jet nozzle diameter, Reynolds number, turbulence intensity and the geometry of the nozzle [6]. Cornaro et al. [8] studied the heat transfer from a convex surface to isothermal impingement jets over a range of Reynolds number ($Re = 6000 - 16000$), jet exit-to-surface spacing ($z/d = 1 - 4$) and cylinder to jet nozzle diameters ($D/d = 2.63 - 5.55$). They concluded that the heat transfer increases with Reynolds number and curvature. The effect of curvature was found to be greater at larger Reynolds number. Tawfek [9] studied the circumferential and radial distribution of Nusselt number for distributions for a range of Reynolds numbers ($Re = 3800 - 40000$), impingement distances ($z/d = 7 - 30$) and curvature ratios ($D/d = 0.06 - 0.14$). It was found that the drop in Nusselt number with increasing radial angle from the impingement points was higher for smaller nozzle to surface distances and smaller jet diameters. An increase in surface curvature was found to increase stagnation Nusselt number values. Wang et al. [10] discussed the heat transfer characteristics of a cylinder in crossflow for a range of curvature ratios ($D/d = 5,1,0.5$) at a jet Reynolds number of 20000. They found that for small cylinders (D/d<0.5) the heat transfer characteristics was similar to that of a cylinder immersed a uniform crossflow and that larger cylinders behaved similarly to that of a flat plate. It was also found that inside the potential core region of the jet, where the centerline velocity of the jet is unchanged, the stagnation heat transfer was found to be higher for smaller cylinders whereas, outside the potential core, larger cylinders provided higher stagnation heat transfer. Lee et al. [11] studied the effects of a convex surface curvature on the local heat transfer of a round impingement jet for a range of distances ($z/d = 3.1 - 4.2$) and Reynolds number ($Re = 11000 - 50000$). They reasoned that the increase in stagnation Nusselt number with increasing curvature was because of the increased acceleration from the stagnation point for higher curvature. The maximum stagnation Nusselt number was found to be within $z/d = 6 - 8$. Balasubramanium [12] studied the effects of impinging distances for isothermal and non-isothermal impinging jets. It was found that heat transfer

was influenced by impinging distances, temperature and turbulence characteristics of the jet. Stagnation Nusselt number was found to match closely for both isothermal and non-isothermal jets at a fixed Reynolds number. The Frossling number distribution over the front portion of the cylinder ($\theta = 0^o - 90^o$), based on the local centerline impinging temperature, was also found to be similar for both isothermal and non-isothermal jets at $z/d = 4,8$. Very little literature was found for large isothermal jets impinging on small cylinders ($D/d < 1$) and the circumferential variation of Frossling numbers with Reynolds numbers for such cases.

2.3. Background on thermal comfort and effect of wind/large jets on human body

Human thermal comfort is affected by external environmental conditions, clothing and physical activity. According to the definition by ASHRAE, thermal comfort is a subjective response or condition of mind that expresses satisfaction with the surrounding thermal environment [13]. This standard is based on Fanger's "comfort equation", a heat balance model of a human body [14]. This method suggests calculation of a Predicted Mean Vote (PMV) index for identifying the thermal comfort of an environment based on six different parameters: air temperature, air velocity, mean radiant temperature, humidity, clothing and activity. This index varies between -3 for cold to +3 for hot. Another index named Predicted Percentage Dissatisfied (PPD) measures the degree of discomfort, predicts the percentage of people dissatisfied with the environment conditions, and the index value varies between 5% and 100%. However, these methods do not measure the heat flux directly but instead estimate it empirically, using temperature and other environmental conditions. A heat flux sensor, on the other hand, can be used to measure the heat flux from different parts of a human body directly. A heat flux sensor can also be integrated into a wearable electronic device to connect to the air-conditioning system, thus, helping personalize air conditioning.

There are several computational and experimental studies done on heat transfer from a human body to external environments under natural convection and convective flow of air over the entire body or a thermal manikin [15][16][17][18]. Richard De Dear et al. [19] studied heat transfer from different body segments of a thermal manikin under natural and forced convection. The speed of uniform flow of air for this study

ranged from $0-5\ m/s$. A radiative heat transfer coefficient of 4.5 $W/m^2/K$ was obtained. Hands, feet and peripheral limbs were found to have higher convective heat transfer coefficients than the central torso region. Li et al. [20] studied the effects of strong convective flow on the human body. Computational studies were also done and validated. It was found that the convective heat transfer coefficient of a human body varied as the square root of the wind velocity for high velocities ($1.08 - 12.67$ m/s). The convective heat transfer varied from 16.73 W/m^2/K for a velocity of 1.08 m/s to 71 W/m^2/K for a velocity of 12.67 for a frontal flow against the manikin.

No literature has been found on the study of heat transfer from a human arm to an isothermal impingement jet and study of comparison of heat transfer measurements using an IR camera and a heat flux sensor for low heat flux input to a cylindrical surface. For the current study, heat transfer from a model cylinder to an isothermal cylindrical impingement jet of cylinder to jet diameter ratio of 0.6 for impingement distances ($Z/d = 4{,}8$) to replicate the heat transfer from a real human forearm and to compare the results with results from previous studies. The experiments were conducted at high Reynolds numbers ($Re = 43500$) and heat flux input to the cylinder ($q''_{in} = 1000 W/m^2$) and was measured using both an IR camera and a heat flux sensor. Impingement jet heat transfer studies on the cylinder were later conducted at reduced heat flux input ($q''_{in} = 150\ W/m^2, 200\ W/m^2$) and Reynolds number ($Re = 17000, 31000$), calculated based on heat transfer from a human hand to natural convection, to compare the performance of the IR camera and heat flux sensors at low heat flux input and Reynolds numbers. Studies on the circumferential variation of heat transfer from a human forearm to isothermal jets over a range of Reynolds number ($Re = 9500 - 41000$) and impinging distances of four to eight jet diameters were also done. The results were compared with that obtained using natural convection. Further, empirical relations for variation of stagnation Nusselt number and average Nusselt number with Reynolds number were obtained with very high correlation.

3. Experimental Setup and Apparatus details

3.1. Axial fan and wind tunnel for jet impingement

An example of the experimental setup is shown in figure 2. An isothermal jet of diameter, 'd' was impinged on a uniformly heated cylinder of diameter 'D' at a distance 'z' from the nozzle opening. The impingement jet was generated using an axial fan wind tunnel. The DC powered fan draws in air at room temperature from the surroundings. The speed of the fan is controlled by varying the input voltage to the fan. The axial fan is powered by a TekPower 30V, 10A DC Power source. The inner diameter of the wind tunnel is 12.9 cm and is 167.6 cm length. Flow straighteners are placed inside the wind tunnel at a distance of 122 cm from the fan to straighten any rotational component of velocity of air inside the wind tunnel. In addition, fiberglass screen meshes are also placed in the wind tunnel at a distance of 30.5, 81.3 and 168 cm from the fan to break the formation of boundary layers and make the axial velocity uniform. Velocity at the end of the wind tunnel was measured using a pitot tube fitted manometer (Dwyer Mark II).

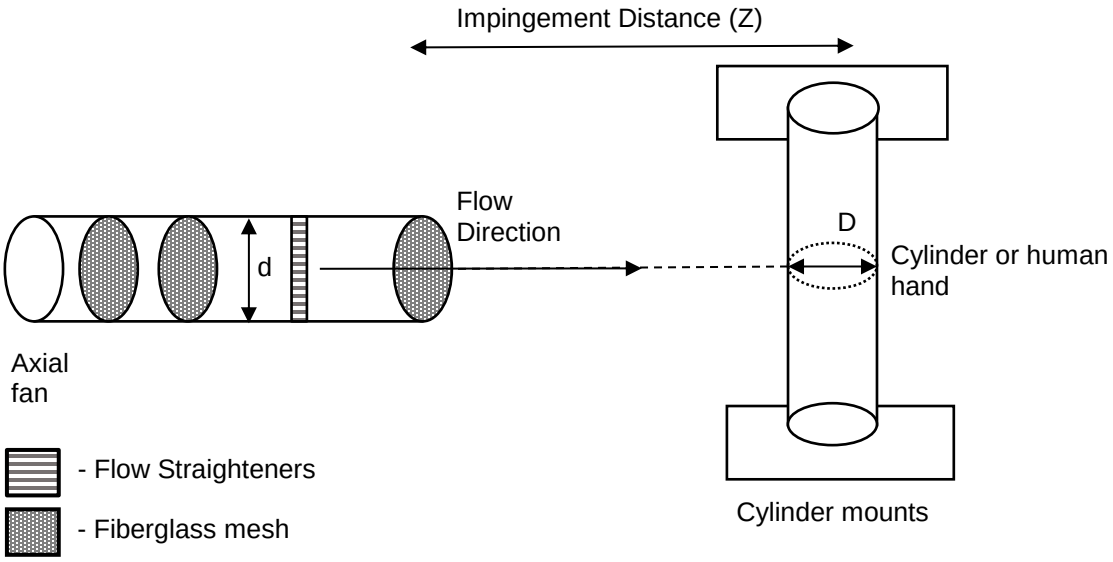

Figure 2: Experimental setup for impingement studies on a cylinder and a human forearm

3.2. Cylinder construction

To mimic the dimensions of a human hand, a PVC cylindrical pipe of diameter 7.32 cm was used for the experiments. The cylinder has a total length of 66.55 cm and has a thickness of 0.61 cm. A 25.66 cm long, 60Ω aluminum backed resistance heater was wrapped around the pipe and stuck on using a 3M permanent double sided tape. The aluminum foil backing ensures uniform distribution of heat flux across the surface of the cylinder. A 1.91 cm thick foam insulation was inserted inside the PVC pipe to provide additional insulation to minimize radial heat loss. The heater was coated with a thin layer of Aervoe Z635 Black Zynolyte High Temperature Paint with a measured emissivity of 0.94 (to simulate the behavior of an actual human hand's emissivity) [21]. Previous research has shown the emissivity of the human skin to be in the range 0.95-0.97 [15][22][19][23]. The overall diameter of the cylinder including the heater was measured to be 7.44 cm. The heater was connected to a Model SC-10 T AC Variac with a maximum rating of 2kW when power in the order of 1000W/m^2 was supplied. For lower power input, a HP Model 6220B DC power supply was used. A Hewlett Packard Model 3468A Multimeter was used for reading the supplied voltage and measuring the resistance of the heater. A Texas Instrument Launchpad with a custom shield to amplify the incoming signals was used for measuring the temperature and heat flux from thermocouples and heat flux sensors. Figure 3 shows the cross section of the cylinder and the detailed view of the construction.

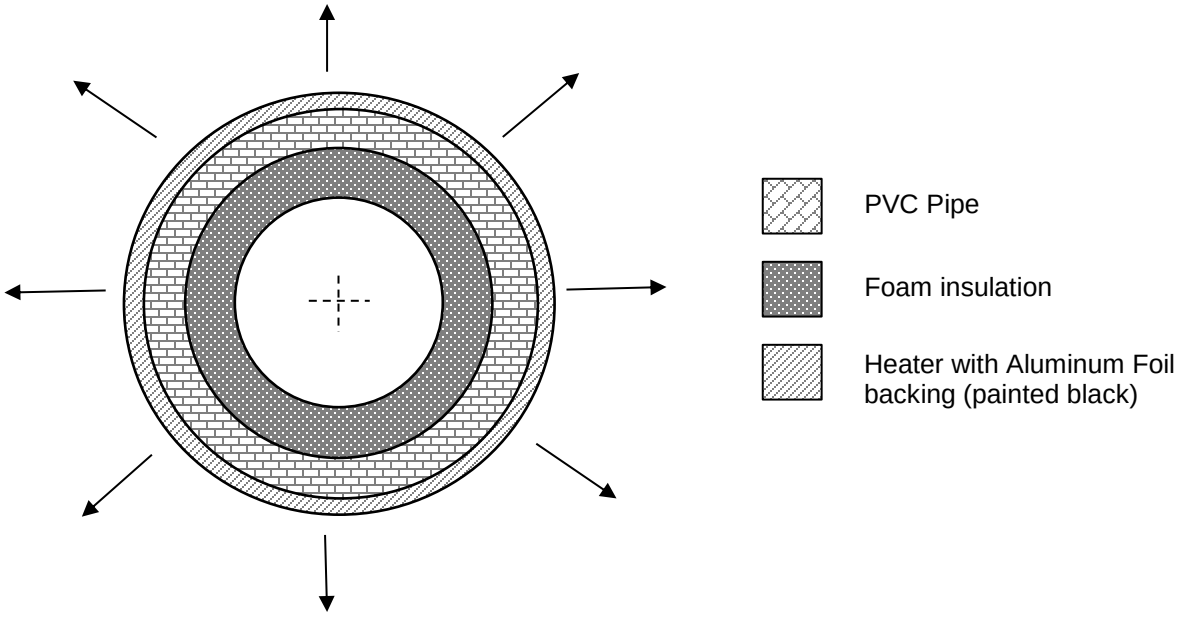

Figure 3: Cross-sectional view of the model cylinder

3.3. IR Camera and Heat Flux Sensor

A FLIR A655SC IR Camera was used to obtain the circumferential temperature distribution of the heated cylinder through FLIR Tools software. The camera has a measurement range of -40 to 150^{o}C with an accuracy of ±2% and has an image resolution of 640x480 pixels. Data from the camera was streamed to a computer system using Gigabit Ethernet cable, and was visualized and processed using FLIR tools software. Detailed studies on uses of IR camera for heat transfer measurements can be found in a number of reviews [24][25][26]. The camera was mounted on an articulating arm, to allow for rotation and adjustment of its position relative to the cylinder. The camera was calibrated using a T-type thermocouple. In later experiments, a 2.54 cm x 2.54 cm Fluxteq PHFS-01 printed thin-film heat flux sensor with an embedded T-type thermocouple was used to measure the temperature and heat flux from the surface to the surroundings. Previous studies suggest that there are significant errors in temperature readings using an IR camera at surface angles greater than 60^0 from the normal viewing angle to the IR camera [24][27]. These errors are a result of directional emissivity of a surface. The quantification of the range of IR camera viewing angle for accounting the directional emissivity of curved surfaces is detailed in Appendix D. For the current experiments, the IR camera was fixed at an angle of 45^0 with respect to the stagnation point

($\theta=0^0$) to measure surface temperatures on the front of the cylinder ($\theta=0^0$ to 90^0). The IR camera was then placed at an angle 135^0 from the stagnation point to measure the surface temperature of the rear portion ($\theta=90^0$ to 180^0). Figure 4 shows the placement of the IR camera relative to experimental setup in figure 2.

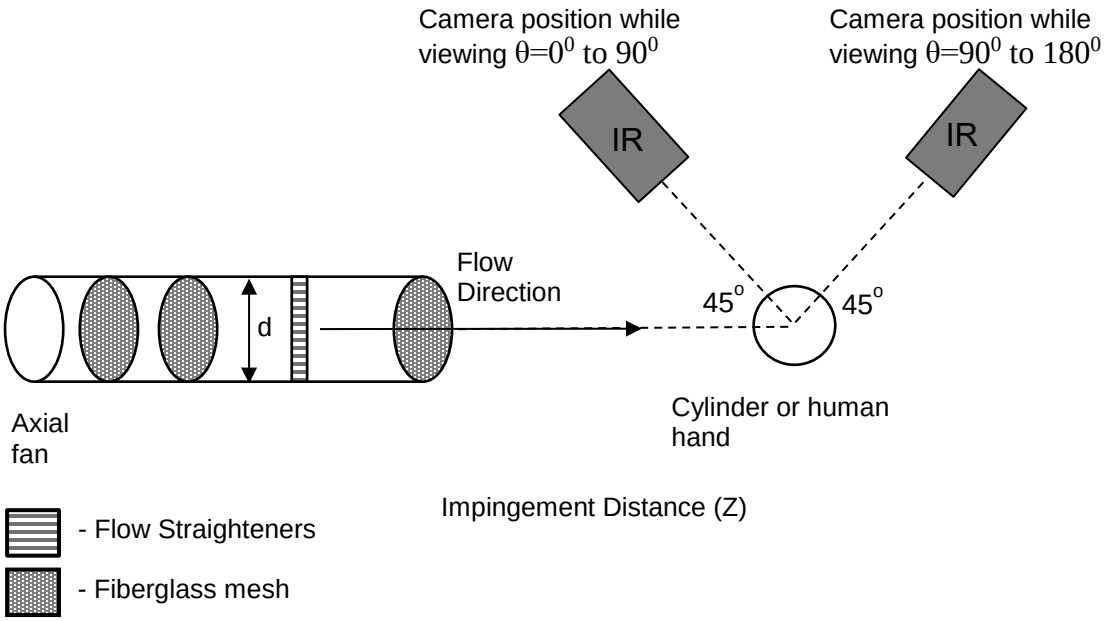

Figure 4: Positions of IR camera for temperature measurements

For experiments using a sensor for measuring the heat flux and temperature of the cylinder, Fluxteq PHFS-01 model heat flux sensors [28] were used. The sensors were calibrated to ASTM C1130 standard. The calibration process involves using a guarded plate apparatus and uses a NIST traceable piece of insulation. The 6.35x8.9 cm rectangular heat flux sensor was pasted onto the outer surface of the heater using a 3M double-sided adhesive tape. A sensor with a sensitivity value of 0.617 $\mu V/W/m^2$ was used for experiments on the comparison of results from the IR camera and the sensor. For experiments on natural convection, a sensor with a sensitivity of 0.85 $\mu V/W/m^2$ was used. Experiments on heat transfer to impingement jets from a human forearm were done using a sensor with a sensitivity of 1.02 $\mu V/W/m^2$. In order to measure the angular displacements from the stagnation point, a paper grid was placed on the cylinder's surface and the grid vortices were marked on the IR camera. The angular displacement between successive points was 5^0. Appendix C details the construction of the paper grid used for angular measurements.

3.4. Natural convection experimental setup

Experiments on measuring the heat flux and temperatures of a normal clothed human forearm and experiments to measure heat transfer from a human hand to the impingement jet were conducted with the help of a male Virginia Tech student. Heat flux sensors were used to measure the heat flux and temperatures. The emissivity of the skin was taken to be 0.96. The experimental setup as shown in figure 5 was used to conduct natural convection experiments on the prototype as well as a human forearm. A controlled environment was used to limit the influence of external disturbances. A cuboidal enclosure made of polythene plastic material was used for the experiments. The enclosure was supported around the edges by wooden bars. It was ensured that there is no significant heating of air inside the enclosure while performing experiments. Wooden mounts were placed at the center of the enclosure to ensure the free flow of air around the cylinder and the hand placed on these mounts. Temperature and heat flux measurements were obtained using a heat flux sensor. The angle $\theta = 0^0$ was taken to be with respect to a level horizontal ground to maintain consistency with the angle $\theta = 0^0$ for experiments using impingement jets. For each experiment, five measurements were taken at a uniform interval of 45^0 from $\theta = -90^0$ to $\theta = 90^0$ because the sensor covered an angle of about 30^0.

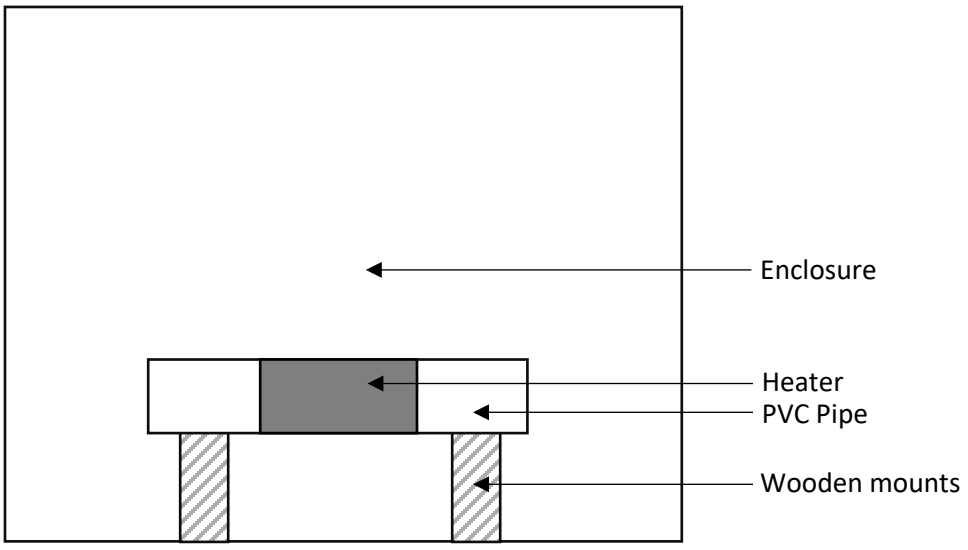

Figure 5: Setup for controlled natural convection experiments

Experiments on heat transfer to impingement jets from a human forearm were also conducted. Unlike the model cylinder, the heat flux from a human arm is not known and varies over long time periods, thus necessitating the use of a heat flux sensor for measuring the heat flux. The heat flux sensor described earlier was pasted on the forearm using a double-sided adhesive tape. The wooden mounts used for holding the cylinder was used to hold the arm in position in front of the impingement jet. The forearm with the sensor was rotated to change the angle of the sensor with respect to the stagnation point. The diameter of the forearm at the location of the sensor was 8.1 cm. The axial fan wind tunnel as described earlier was used for generating the jet for impingement on the forearm.

4. Data Reduction and Uncertainty Analysis

For experiments done using the uniformly heated cylinder, the heat input to the cylinder (q''_{in}) can be calculated as shown in equation 1.

$$q''_{in} = \frac{V^2}{RA} \tag{1}$$

Where V is the supplied voltage, R is the resistance of the heater and A is the surface area of the heater. The net heat flux convected (q''_{conv}) from the cylinder to the impingement jet can be found using the energy balance equation as shown in equation 2.

$$q''_{conv} = q''_{in} - q''_{rad} - q''_{cond,r} - q''_{cond,s} \tag{2}$$

Where, q''_{in} is the net power input to the heater given by equation 1, q''_{rad} is the radiative heat loss to the surroundings given by equation 3.

$$q''_{rad} = \varepsilon\sigma(T^4 - T_{\text{inf}}^4) \tag{3}$$

Where ε is the emissivity of the surface, σ is the Stfan-Boltzmann constant ($= 5.68 * 10^{-8}$), T is the local surface temperature in Kelvin and T_{inf} is the temperature of the surrounding air. $q''_{cond,r}$ is the radial conduction losses through the rear of the cylinder given by equation 4.

$$q''_{cond,r} = \frac{T - T_{inf}}{\pi D(R_{PVC} + R_{insulation})} \tag{4}$$

Where, R_{PVC} is the thermal resistance of the PVC pipe and $R_{insulation}$ is the thermal resistance of the insulation foam. $q''_{cond,s}$ in equation 2 is the heat flux correction due to circumferential conduction through the Aluminum foil, caused by the temperature difference along the circumference of the cylinder. This term can be calculated using a 1-D heat conduction equation along the thickness of the cylinder, as shown in equation 5.

$$q''_{cond,s} = -k_{Al}t_{Al}\frac{\partial^2 T}{\partial s^2} \tag{5}$$

Where, k_{Al} is the thermal conductivity of the aluminum foil and t_{Al} is the thickness of the foil and s denotes the direction along the circumference of the cylinder. The above equation was solved by curve fitting a sixth order polynomial on a plot of local temperature versus the location along the circumference, taking $s = 0$ to be the stagnation point to obtain the second derivative of the temperature with respect to its circumferential location. The local convection heat transfer coefficient (h_c) and the Nusselt number (Nu) at each location can be found as shown in equations 6 and 7.

$$h_c = \frac{q''_{conv}}{T - T_{inf}} \tag{6}$$

$$Nu = \frac{h_c D}{k_{air}} \tag{7}$$

Where, k_{air} is the thermal conductivity of air. For a cylinder in cross flow, the local Frossling Number is defined as the ratio of the local Nusselt number and the square root of the Reynolds number of the flow. As shown in equation 8.

$$Fr = \frac{Nu}{\sqrt{Re_D}} \tag{8}$$

Where Re_D is the Reynolds number calculated based on the cylinder diameter, D, jet velocity at the nozzle exit, v_0 and kinematic viscosity (ν) at film temperature ($Re_D = v_0 D/\nu$). The average Frossling number was obtained by numerically integrating the local Frossling number over the circumference of the cylinder ($\theta=0^0$ to 180^0).

For experiments on the prototype using a heat flux sensor, the convective heat flux can be obtained using equation 9.

$$q''_{conv} = \frac{V}{S} - q_{rad}'' \tag{9}$$

Where V is the voltage measurement from the sensor and S is the sensitivity in V/W/m^2. The Nusselt number and Frossling number can be found using the previous equations 5 and 6. The temperature measurements were obtained using a T- type thermocouple embedded in the sensor.

Experimental uncertainty for all experiments conducted was calculated using the method laid out by Moffat [29]. A detailed explanation on calculation of the uncertainty of Frossling number and uncertainty of the instruments used for measuring temperatures, heat fluxes and velocities have been included in Appendix A. Uncertainty for each set of experiments have been discussed in the results section.

5. Results and Discussion

5.1. Variation of centerline velocity

Figure 6 shows the variation of centerline velocity of the jet (v_j) with distance from the jet nozzle exit at $Re = 45000$. The values of jet velocity have been normalized with respect to the jet velocity at the exit of the nozzle (z=0) and the distance has been normalized with respect to the nozzle diameter. The centerline velocity remains constant from a distance of $z/d = 0$ until $z/d = 4$. There is a steady drop in centerline velocity from $z/d = 8$ until $z/d = 16$. This suggests that the potential core region of the jet ends at distance between $z/d = 4$ until $z/d = 8$. The reduction of the centerline velocity from z/d=8 to z/d=16 can be attributed to the increasing entrainment effect of the surrounding stagnant air. The jet centerline velocity was found to decrease with the inverse of distance. The values of normalized centerline velocity of an isothermal impingement jet match very well with the results obtained by Balasubramanian [12] and Malmström et al. [30] to within the bounds of estimated uncertainties shown in figure 6.

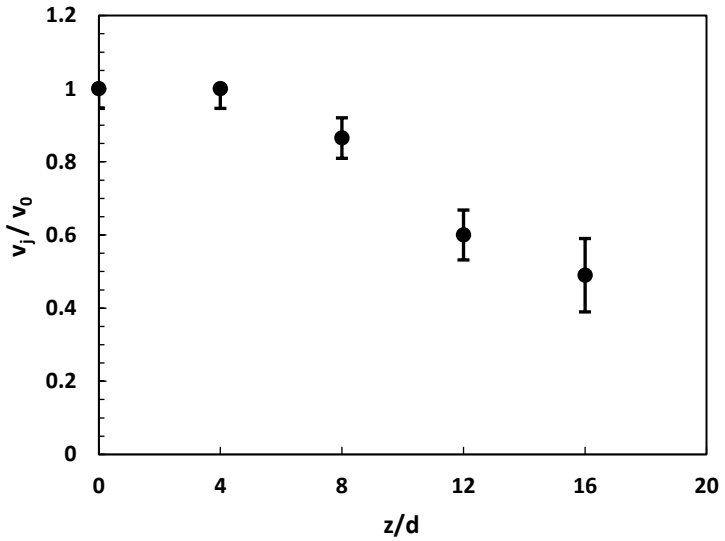

Figure 6: Centerline jet velocity variation with distance from nozzle (Re=43500)

5.2. Local Frossling number distribution around the cylinder circumference in a jet flow

Figure 7 shows the variation of Frossling number along the circumference of the cylinder for Reynolds number of 43500 at normalized distances, $z/d = 4$ and $z/d = 8$ using the IR camera. The local Frossling number, irrespective of impingement distance tends to decrease with increasing angle with respect to the stagnation point until $\theta = 90^0$ to $\theta = 120^0$, due to the growth of thermal boundary layer. For angles greater than $\theta = 120^0$, there is a gradual increase in the heat transfer caused by reverse periodic vortices, after reattachment of free shear layer [31]. Further, the heat transfer from the cylinder at all angles is larger for $z/d = 8$ compared to $z/d = 4$. This can be attributed to an increase in turbulence of the impingement jet due to increasing entrainment effect of the surrounding stagnant air [12]. The heat transfer distribution for $z/d = 4$ matches well with the results obtained by Sanitjai and Goldstein [32] with a maximum of 10% difference in the circumferential Nusselt number distribution. They performed heat flux measurements on a uniformly heated cylinder immersed in a crossflow from an impingement jet from a rectangular nozzle, over a wide range of Reynolds numbers at an impinging distance of $z/d = 5$. The Frossling number variation for both impingement distances also matches closely with the results obtained by Balasubramanium et al. [12] to within 6% difference. The estimated average uncertainty in the measurement of Frossling number was found to be around 4.4% for $Re = 43500$, $z/d = 4$ and $z/d = 8$.

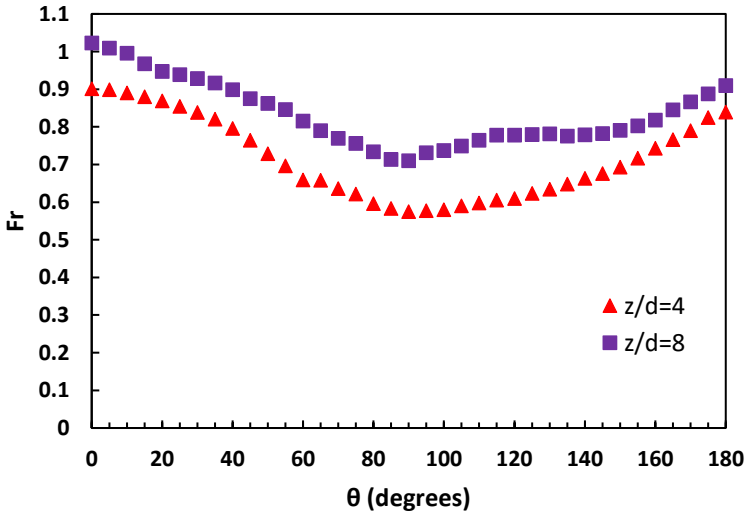

Figure 7: Variation of Frossling number along the circumference in a jet flow (Re=43500)

5.3. Comparison of heat transfer results from heat flux sensor and IR camera

Figure 8 shows the variation of local Frossling number along the circumference of the cylinder for a jet Reynolds number of 43500, using both a heat flux sensor and the IR camera. The measurements were taken simultaneously using both the sensor and the IR camera. Figure 8 also includes the variation of local Frossling number calculated using only temperature measurements from the thermocouple embedded in the sensor. Frossling numbers using this method were calculated using equations developed for Frossling number calculations using an IR camera (equations 1-6).

It can be observed that although the Frossling number plot for all three cases match well for angles from $\theta = 0^0$ to $\theta = 70^0$ and from $\theta = 120^0$ to $\theta = 180^0$, the curvature of the Frossling number variation found using the heat flux sensor is more than that found using the IR camera. The reason for mismatch of the Frossling numbers variation in the range $\theta = 70^0$ to $\theta = 120^0$ can be attributed to the fact that the heat flux sensor averages the heat flux over its area, which covers an angle of 30^0 along the circumference of the cylinder. This averaging effect leads to values lower than actual value at any given point for a concave curve. This can be confirmed using the third curve found using the thermocouple in the heat flux sensor, which measures the temperature of a point rather than averaging. The estimated average uncertainty for calculating the Frossling number using the IR camera was 4.4%, 3.9% using the heat flux sensor and 4.3% using the thermocouple. Uncertainty in the velocity measurements were found to be the major contributor to the uncertainty in Frossling number whereas uncertainty in temperature measurements were found to be major contributor to uncertainty in the calculation of Nusselt numbers. The reduction in temperature due to placement of sensor was found to be 0.6^0C when compared with the results obtained using the IR camera. This translates to a 4% change in temperature difference due to placement of the sensor. Since the convective heat flux and the Frossling number is varies directly with the temperature difference, the change in Frossling number due to placement of sensor is also 4% which matches with the calculated estimated uncertainty of the Frossling number.

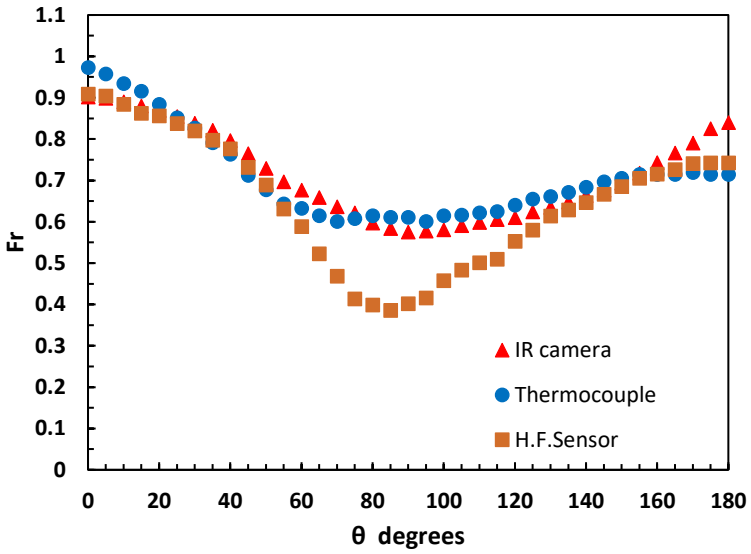

Figure 8: Comparison of circumferential variation of Frossling number (z/d=4, Re=43500)

Since a human hand has a much lower heat flux than the heat input provided to the model cylinder in the previous experiments, jet impingement studies were also conducted at reduced input heat flux values ($q''_{in} = 150\ W/m^2$ and $200\ W/m^2$). Olesen [23] tabulated results from a number of sources on comfort conditions for different national-geographic groups, different sexes and age groups. It was found that the preferred ambient temperature varied between 25±1^{0}C and the preferred skin temperature varied between 33±1^{0}C. Therefore, Reynolds numbers for these input heat flux values were calculated based on the average Frossling number from previous results, assuming a final comfort skin temperature to be 32^{0}C and an ambient temperature of 25^{0}C. The Reynolds number thus used for $q''_{in} = 150\ W/m^2$ was found to be 17000 and for $q''_{in} = 200\ W/m^2$ was found to be 31000. Two experiments were done for each pair of q''_{in} values. Figure 9 show the results obtained using both an IR camera and a heat flux sensor for $150\ W/m^2$ and $200\ W/m^2$ respectively. The Frossling number variation calculated using measurements from a heat flux sensor matches closely with that of an IR camera. The estimated uncertainty in the calculation of Frossling number using the IR camera was found to be 10.8% for $Re = 31000$ and 16.5% for $Re = 17000$, and was 7.5% for $Re = 31000$ and 13.5% for $Re = 17000$ using the heat flux sensor. Since the heat flux calculation using an IR camera depends on the temperature difference between the heated surface and the ambient

surroundings, the lower temperature difference (~4^0C) for the set of experiments when compared to the previous experiments (~18^0C) leads to greater uncertainty. The heat-flux sensor measures heat flux directly and so the uncertainty in measuring the Frossling number values do not increase as much as the IR camera at reduced input heat flux. Moreover, measurement of heat flux from a human arm using an IR camera requires the knowledge of total heat flux output from the forearm, which changes significantly depending on the metabolic rate of the person[15,23]. Thus, for experiments involving low temperature differences, the heat flux sensor was used instead of an IR camera.

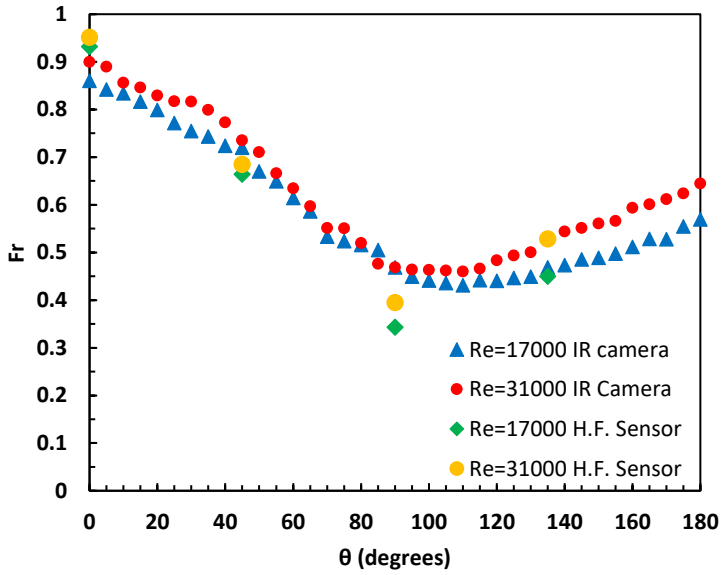

Figure 9: Comparison of circumferential Frossling number variation around a cylinder in a jet using an IR camera and a heat flux (H.F.) sensor (z/d=4, Re=17000, 31000)

5.4. Circumferential variation of Frossling number on a human forearm in a jet

Figure 10.a and 10.b show the variation of Frossling number along the circumference of a human forearm for a range of Reynolds number: 9500, 13750, 17000, 31000 and 43500 at a normalized distance of $z/d = 4$ and $z/d = 8$, respectively, using a heat flux sensor. The local Frossling numbers, irrespective of Reynolds numbers tend to decrease with increasing angle with respect to the stagnation point until $\theta = 90^0$ to $\theta = 120^0$, due to growth of the thermal boundary layer. From $\theta = 120^0$ to $\theta = 180^0$, There is a steady increase in the heat transfer rate from the cylinder to the jet. This increase could be explained in a similar

manner as was done for the uniformly heated cylinder earlier [31]. Further, the decrease in local Frossling number with the Reynolds number near the flow separation region, between the angles, $\theta = 90^0$ to $\theta = 120^0$, found to be more at $z/d = 8$ than $z/d = 4$ and vice versa for the backside of the cylinder ($\theta = 135^0$ to $\theta = 180^0$).

It was also found that the average Frossling number at $z/d = 8$ was greater than at $z/d = 4$ for all Reynolds numbers as shown in figure 11. A 56% increase in average Frossling number between Reynolds numbers 9500 and 41000 was obtained. The rate of increase of the average Frossling number for $z/d = 8$ was found to be slightly greater than that for $z/d = 4$. The Frossling number variation matches well with the results obtained with the uniformly heated cylinder. According to the uncertainty analysis method provided in Moffat [29], the average estimated uncertainty and the average uncertainties of Frossling number values under 95% confidence interval for the individual experiments at 4D and 8D are as tabulated in Tables 1 and 2. The large difference between the uncertainty between Nusselt number and the Frossling number is because of the uncertainty in Reynolds number increases with decreasing speed.

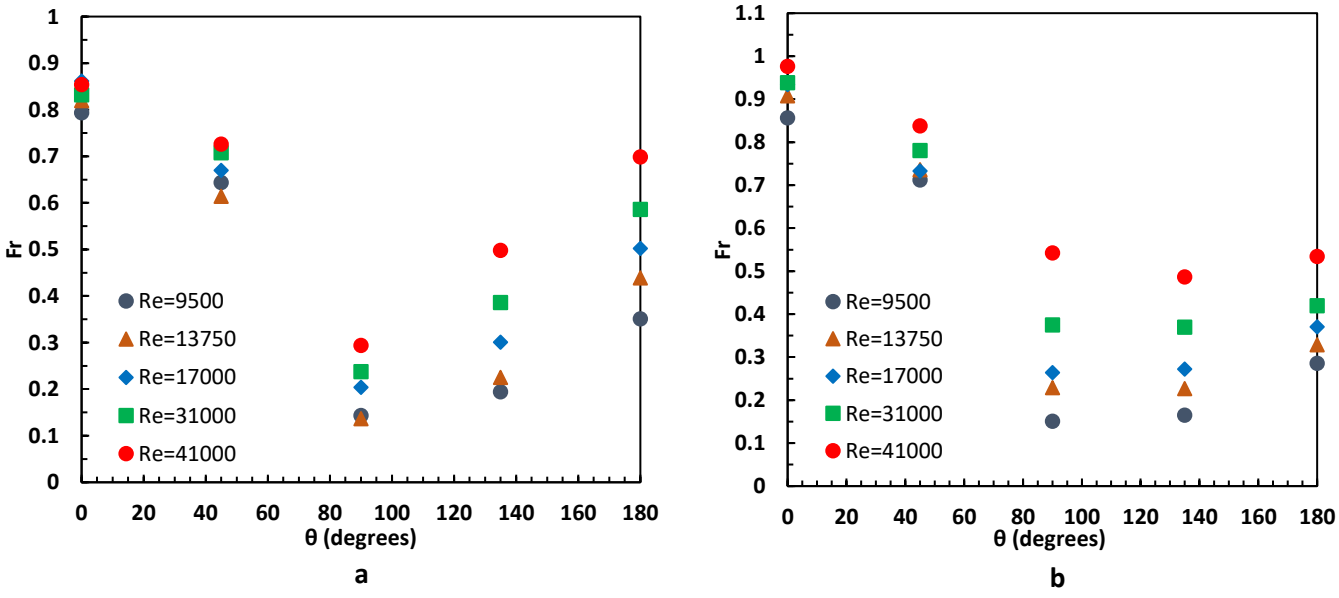

Figure 10: Circumferential variation of Frossling number for different jet Reynolds number at a) z/d=4 and b) z/d=8

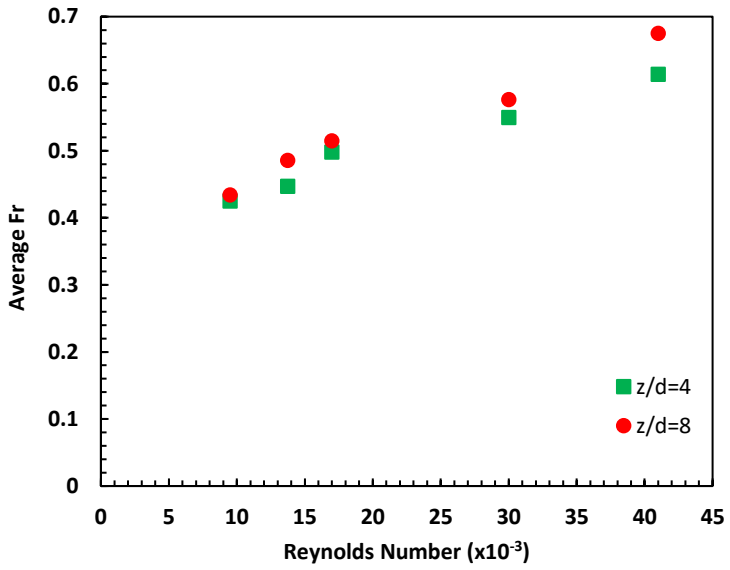

Figure 11: Variation of average Frossling number of a forearm with Reynolds number of the jet at z/d=4 and 8

Table 1: Uncertainties in calculation at z/d=4 for different Reynolds numbers

Re	Estimated Uncertainty (%)			95% CI for Fr (%)
	Fr	Nu	h_c	
9500	25.01	2.04	2.4	2.58
13750	15.88	1.52	1.76	1.87
17000	12.91	1.35	1.56	1.25
30000	6.29	0.9	1.2	1.13
41000	4.85	0.85	1	0.93

Table 2: Uncertainties in calculation at z/d=8 for different Reynolds numbers

Re	Estimated uncertainty (%)			95% CI for Fr (%)
	Fr	Nu	h_c	
9500	25	2.35	2.72	2.25
13750	15.8	1.58	1.88	1.49
17000	14.33	1.09	1.27	1.56
30000	6.29	0.86	0.9	0.97
41000	4.83	0.57	0.74	0.85

5.5. Measurement of heat transfer under natural convection

A detailed circumferential variation study on natural convection (N.C.) on the forearm was done using a heat flux sensor on the backside of the forearm. Twenty experiments on the forearm were conducted in an open environment setting, twenty experiments were conducted under the controlled environment described in the section on experimental setup and fifteen experiments were conducted on the heated cylinder under the controlled environment for comparison. As previously mentioned, the angle $\theta = 0^0$ was taken to be with respect to a level horizontal ground. The heat transfer results from the individual experiments for all three cases are shown in Appendix F. Figure 12 shows a combined result of the circumferential variation of convective heat transfer coefficient for a human forearm. The convective heat transfer coefficient averaged over the circumference ($h_{c,avg} = 3.32\ W/m^2/K$) match the result obtained by Churchill and Chu [33] on a cylinder under natural convection ($h_{c,avg} = 3.35\ W/m^2/K$). The general trend of the curves is a nearly constant heat transfer coefficient value from $\theta = -90^0$ to $\theta = -45^0$ and then a gradual decrease in the value from $\theta = -45^0$ to $\theta = 90^0$. The circumferential variation of convective heat transfer coefficient match well between the human forearm and the heated cylinder.

The convection heat transfer and uncertainty in the open environment were found to be more than the results obtained from the control environment. Small wafts of air, resulting from external disturbances, increases the heat transfer coefficient and its variation in an open environment. The uncertainties of convection heat transfer coefficient values under 95% confidence are 9.2% for experiments on the forearm in a control environment, 32.6% for experiments on the forearm in an open environment, 17.7% for experiments on the cylinder in a control environment. The maximum variation in measurements was found to be at 90^0 for all three cases.

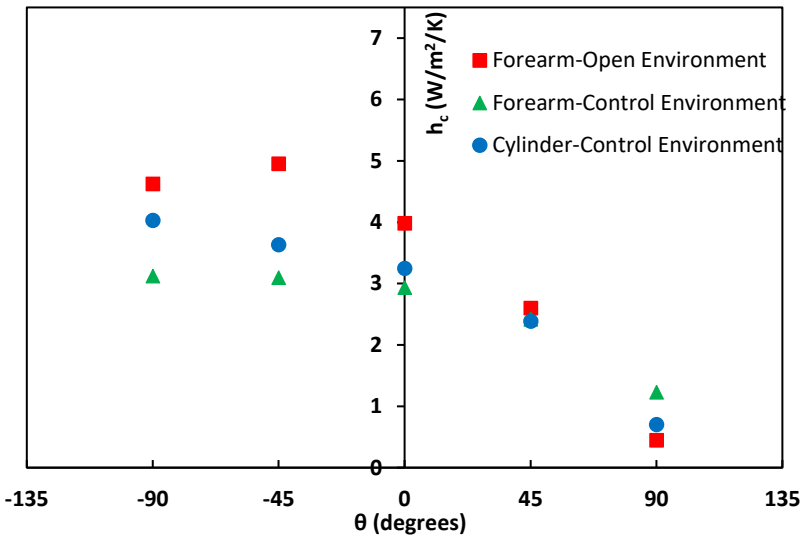

Figure 12: Circumferential variation of convection heat transfer coefficient of a forearm and a cylinder under natural convection for open and control environment

Figure 13 shows the comparison of convection heat transfer coefficient averages over the circumference of the human forearm over a range of jet velocities and due to natural convection. It can be observed that there is a significant improvement in heat transfer using impingement jets when compared to heat transfer by natural convection. A nearly four-fold increase in convection heat transfer coefficient was obtained for a jet velocity of 2 m/s when compared with that under natural convection in an open environment and a five-fold increase compared to natural convection in the control environment.

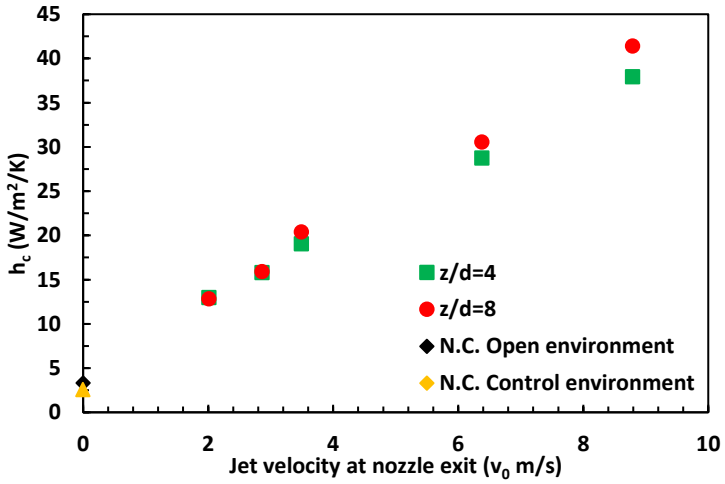

Figure 13: Variation of average convection heat transfer coefficient of a forearm with jet velocity at z/d=4 and 8

5.6. Correlations for estimating heat transfer to large isothermal jets

5.6.1. Variation of stagnation Nusselt number with Reynolds number

Figure 14 shows the variation of stagnation point Nusselt number with Reynolds number of the heated cylinder using a heat flux sensor at $z/d = 4$. The overall convective heat transfer in terms of Nusselt number around a circular cylinder is typically correlated by a power law relationship (equation 10)

$$Nu = C.Re^{m} \tag{10}$$

Based on this equation, a curve fit analysis was performed and the values of C and m were found to be 0.458 and 0.571 with an R^2 value of 0.97 (equation 11). The Nusselt number values obtained using this correlation is in good agreement with the values obtained using the correlation found by Sanitjai and Goldstein [32], who obtained the power coefficient in equation 10 to be 0.5.

$$Nu = 0.477Re^{0.567} \tag{11}$$

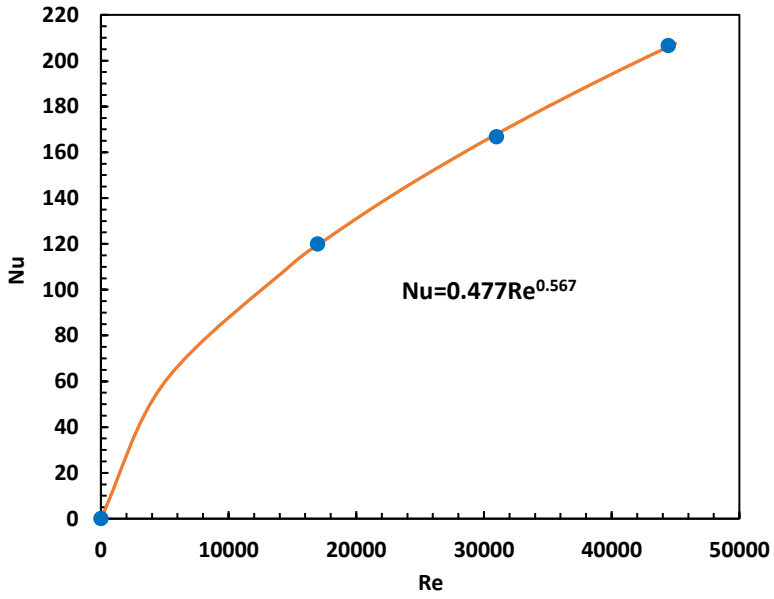

Figure 14: Variation of stagnation Nusselt number with Reynolds number for a heated cylinder (z/d=4)

Figure 15.a and 15.b show the variation of stagnation Nusselt number with Reynolds number of a human forearm using a heat flux sensor at $z/d = 4$ and $z/d = 8$, respectively with $R^2 = 0.99$. The curve fit analysis of the power law equation for these results gives equations 12 and 13. The stagnation Nusselt

number was found to be greater for $z/d = 8$ than $z/d = 4$ as was found in the uniformly heated cylinder at $Re = 43500$.

$$Nu = 0.6Re^{0.533} \quad (12)$$

$$Nu = 0.28Re^{0.618} \quad (13)$$

The power coefficient of stagnation Nusselt number correlation obtained for a human forearm matches the coefficient obtained using the heated cylinder to within 5%.

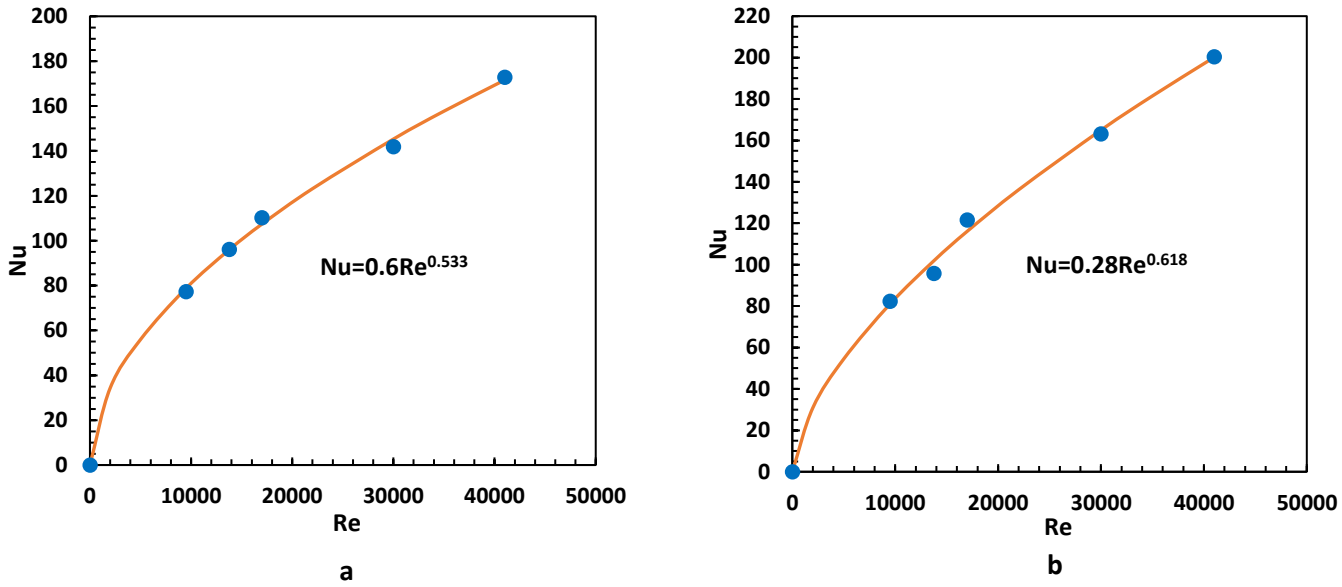

Figure 15: Variation of stagnation Nusselt number with Reynolds number for a human forearm at a) z/d=4 and b) z/d=8

5.6.2. Variation of average Nusselt number with Reynolds number for a human forearm

Figure 16.a and 16.b show the variation of circumference averaged Nusselt number with Reynolds number of a human forearm using a heat flux sensor at $z/d = 4$ and $/d = 8$, respectively. Equations 14 and 15 were found using curve fit analysis and correlated using the power law relationship (equation 10) for $z/d = 4$ and $z/d = 8$, respectively ($R^2 = 0.99$) . It was found that the power coefficient for Reynolds number for $z/d = 4$ was found to be greater than $z/d = 8$. This shows that the circumferential average Nusselt number is greater for $z/d = 8$ than $z/d = 4$ as expected based on higher average Frossling number found earlier.

$$Nu = 0.035Re^{0.767} \quad (14)$$

$$Nu = 0.025Re^{0.809} \quad (15)$$

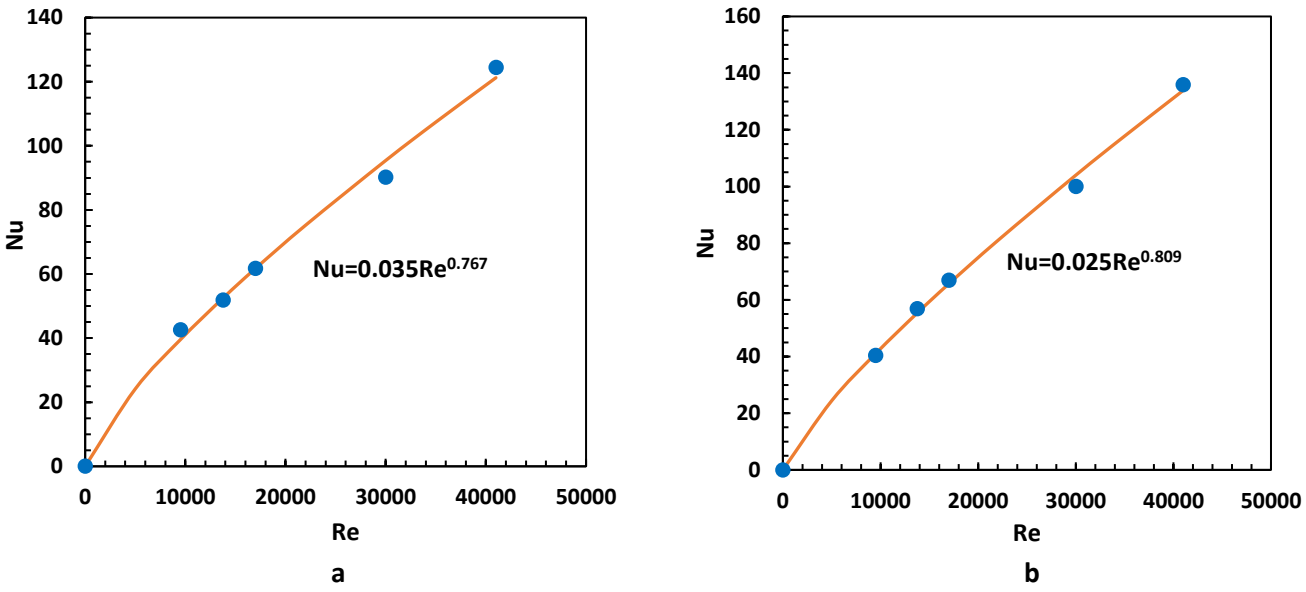

Figure 16: Variation of average Nusselt number with Reynolds number for a human forearm at a) z/d=4 and b) z/d=8

6. Conclusion and Future Scope

6.1. Conclusion

The possibility of use of impingement jets for creation of microenvironment was studied. Centerline velocity distribution of the impingement jet showed that the potential region of the jet was at a distance of $z/d = 4 - 8$. Circumferential variation of heat transfer studied on a model cylinder impinged on by a horizontal isothermal jet at various distances and Reynolds number showed that the Frossling number increases with distance from $z/d = 4$ until $z/d = 8$ at any given point on the cylinder. It was found that use of heat flux sensor led to lower uncertainty when compared to an IR camera at lower heat flux measurements. Further, the study on circumferential variation of heat transfer to isothermal impingement jets was studied on a human forearm showed that there is a significant increase in heat transfer using the jet when compared to natural convection. A five-fold increase in convection heat transfer coefficient was observed between heat transfer through natural convection in a controlled environment and that using an impingement jet at Reynolds number as low as 9500. Empirical correlations for predicting the stagnation and average Nusselt number were developed with high values of correlation coefficients. Overall, it was found that isothermal impingement jets could be used to provide substantial heat transfer over the range of Reynolds number and impinging distances tested and so has significant potential to be used for local thermal comfort and an effective means to build thermally conditioned microenvironments.

6.2. Future Scope

This work focuses on heat transfer from a human arm to large horizontal isothermal jets impinging on it in a transverse direction. This study can leter be extended to other body parts such as the head, legs as well to get a better understanding of the human body in a thermal microenvironment. Comparison of heat transfer from non-isothermal jets to simulate the cold air from an HVAC system with the heat transfer results from isothermal currently obtained can be done and correlations for heat transfer for such flows can also be developed. Impinging directions other than transverse, such as at an oblique angle can also be studied to understand heat transfer from an individual when the individual's orientation is not directly in the transverse

direction of the jet flow. Comparison of the proposed microenvironment creation system with the already existing ones in terms of economic viability, overall energy usage and thermal comfort would help in understanding the benefits and drawbacks of these systems.

References

[1] S.D. Hamilton, K.W. Roth, J. Brodrick, Using microenvironments to provide individual comfort, ASHRAE J. (2003).

[2] K. Tsuzuki, E. Arens, F. Bauman, D. Wyon, Individual thermal comfort control with desk-mounted and floor-mounted task/ambient conditioning (TAC) systems, in: Proc. Indoor Air '99,Volume 2, 1999: pp. 368–373. http://www.escholarship.org/uc/item/06j3k53n.

[3] G. Abramovich, Theory of free turbulence for the case of a submerged jet, Theory Turbul. Jets. (2003).

[4] H. Martin, Heat and Mass Transfer between Impinging Gas Jets and Solid Surfaces, Adv. Heat Transf. 13 (1977) 1–60. doi:10.1016/S0065-2717(08)70221-1.

[5] J.E. Ferrari, N. Lior, J. Slycke, An evaluation of gas quenching of steel rings by multiple-jet impingement, J. Mater. Process. Technol. 136 (2003) 190–201. doi:10.1016/S0924-0136(03)00158-4.

[6] K. Jambunathan, E. Lai, M.A. Moss, B.L. Button, A review of heat-transfer data for single circular jet impingement, Int. J. Heat Fluid Flow. 13 (1992) 106–115.

[7] C. duP. Donaldson, R.S. Snedeker, A study of free jet impingement. Part 1. Mean properties of free and impinging jets, J. Fluid Mech. 45 (1971) 281. doi:10.1017/S0022112071000053.

[8] C. Cornaro, A.S. Fleischer, M. Rounds, R.J. Goldstein, Jet impingement cooling of a convex semi-cylindrical surface, Int. J. Therm. Sci. 40 (2001) 890–898. doi:10.1016/S1290-0729(01)01275-3.

[9] A.A. Tawfek, Heat transfer due to a round jet impinging normal to a circular cylinder, Heat Mass Transf. 35 (1999) 327–333. doi:10.1007/s002310050332.

[10] X.L. Wang, D. Motala, T.J. Lu, S.J. Song, T. Kim, Heat transfer of a circular impinging jet on a circular cylinder in crossflow, Int. J. Therm. Sci. 78 (2014) 1–8. doi:10.1016/j.ijthermalsci.2013.11.005.

[11] D.H. Lee, Y.S. Chung, D.S. Kim, Turbulent flow and heat transfer measurements on a curved surface with a fully developed round impinging jet, Int. J. Heat Fluid Flow. 18 (1997) 160–169. doi:10.1016/S0142-727X(96)00136-1.

[12] K. Balasubramaniam, Experimental Measurements of Heat Transfer from a Cylinder to Turbulent Isothermal and Non-Isothermal Jets, Virginia Polytechnic Institute and State University, 2016.

[13] American Society of Heating Refrigerating and Air Conditioning Engineers (ASHRAE), ANSI/ASHRAE Standard 55: Thermal Environmental Conditions for Human Occupancy., 2013. doi:ISSN 1041-2336.

[14] P.O. Fanger, Calculation of thermal comfort, Introduction of a basic comfort equation, ASHRAE Trans. 73 (1967) III.4.1-III.4.20.

[15] H. Arens, E., Zhang, The skin's role in human thermoregulation and comfort, in: Therm. Moisture Transp. Fibrous Mater., 2006: pp. 560–602. doi:10.1080/09613218.2011.556008.

[16] A. Cross, M. Collard, A. Nelson, Body segment differences in surface area, skin temperature and 3D displacement and the estimation of heat balance during locomotion in hominins, PLoS One. 3

(2008). doi:10.1371/journal.pone.0002464.

[17] C. Huizenga, Z. Hui, E. Arens, A model of human physiology and comfort for assessing complex thermal environments, Build. Environ. 36 (2001) 691–699. doi:10.1016/S0360-1323(00)00061-5.

[18] B. Lin, Z. Wang, H. Sun, Y. Zhu, Q. Ouyang, Evaluation and comparison of thermal comfort of convective and radiant heating terminals in office buildings, Build. Environ. 106 (2016) 91–102. doi:10.1016/j.buildenv.2016.06.015.

[19] R.J. de Dear, E. Arens, Z. Hui, M. Oguro, Convective and radiative heat transfer coefficients for individual human body segments., Int. J. Biometeorol. 40 (1997) 141–156. doi:10.1007/s004840050035.

[20] C. Li, K. Ito, Numerical and experimental estimation of convective heat transfer coefficient of human body under strong forced convective flow, J. Wind Eng. Ind. Aerodyn. 126 (2014) 107–117. doi:10.1016/j.jweia.2014.01.003.

[21] R.J. Cherry, T.E. Diller, C.B. Williams, K.D.T. Ngo, Development of a Novel,Manufacturing Method of Producing Cost-Effective Thin-Film Heat Flux Sensors, Virginia Polytech. Inst. State Univ. (2015).

[22] J.A.J. Stolwijk, MATHEMATICAL MODELS OF THERMAL REGULATION, Ann. N. Y. Acad. Sci. 335 (1980) 98–106. doi:10.1111/j.1749-6632.1980.tb50739.x.

[23] B.. Olesen, Thermal Comfort, 1982.

[24] G.M. Carlomagno, G. Cardone, Infrared thermography for convective heat transfer measurements, 2010. doi:10.1007/s00348-010-0912-2.

[25] H. Thomann, B. Frisk, Measurement of heat transfer with an infrared camera, Int. J. Heat Mass Transf. 11 (1968) 819–826. doi:10.1016/0017-9310(68)90126-9.

[26] T. Astarita, G. Cardone, G.M. Carlomagno, C. Meola, A survey on infrared thermography for convective heat transfer measurements, Opt. Laser Technol. 32 (2000) 593–610. doi:10.1016/S0030-3992(00)00086-4.

[27] T.-Y. Cheng, D. Deng, C. Herman, Curvature Effect Quantificaiton for In-Vivo IR Thermography, Vol. 2 Biomed. Biotechnol. (2012) 127. doi:10.1115/IMECE2012-88105.

[28] PHFS-01 Heat Flux Sensor, (n.d.). http://www.fluxteq.com/phfs-01-heat-flux-sensor (accessed July 28, 2017).

[29] R.J. Moffat, Describing the uncertainties in experimental results, Exp. Therm. Fluid Sci. 1 (1988) 3–17. doi:10.1016/0894-1777(88)90043-X.

[30] T.G. MALMSTRÖM, A.T. KIRKPATRICK, B. CHRISTENSEN, K.D. KNAPPMILLER, Centreline velocity decay measurements in low-velocity axisymmetric jets, J. Fluid Mech. 346 (1997) S0022112097006368. doi:10.1017/S0022112097006368.

[31] S. Sanitjai, R.J. Goldstein, Heat transfer from a circular cylinder to mixtures of water and ethylene glycol, Int. J. Heat Mass Transf. 47 (2004) 4785–4794. doi:10.1016/j.ijheatmasstransfer.2004.05.013.

[32] S. Sanitjai, R.J. Goldstein, Forced convection heat transfer from a circular cylinder in crossflow to

air and liquids, Int. J. Heat Mass Transf. 47 (2004) 4795–4805. doi:10.1016/j.ijheatmasstransfer.2004.05.012.

[33] S. Churchill, H. Chu, Correlating equations for laminar and turbulent free convection from a horizontal cylinder, Int. J. Heat Mass Transf. 18 (1975) 1323–1329. doi:10.1016/0017-9310(75)90222-7.

[34] D. Ding, T. Tang, G. Song, A. McDonald, Characterizing the performance of a single-layer fabric system through a heat and mass transfer model - Part I: Heat and mass transfer model, Text. Res. J. 81 (2010) 398–411. doi:10.1177/0040517510388547.

[35] M.S. Ferreira, J.I. Yanagihara, A transient three-dimensional heat transfer model of the human body, Int. Commun. Heat Mass Transf. 36 (2009) 718–724. doi:10.1016/j.icheatmasstransfer.2009.03.010.

[36] S. Kumar, M.K. Singh, V. Loftness, J. Mathur, S. Mathur, Thermal comfort assessment and characteristics of occupant's behaviour in naturally ventilated buildings in composite climate of India, Energy Sustain. Dev. 33 (2016) 108–121. doi:10.1016/j.esd.2016.06.002.

[37] F.R. D'Ambrosio Alfano, B.W. Olesen, B.I. Palella, G. Riccio, Thermal comfort: Design and assessment for energy saving, Energy Build. 81 (2014) 326–336. doi:10.1016/j.enbuild.2014.06.033.

[38] D.N. Sørensen, L.K. Voigt, Modelling flow and heat transfer around a seated human body by computational fluid dynamics, Build. Environ. 38 (2003) 753–762. doi:10.1016/S0360-1323(03)00027-1.

[39] W. Colban, A. Gratton, K.A. Thole, M. Haendler, Heat Transfer and Film-Cooling Measurements on a Stator Vane With Fan-Shaped Cooling Holes, J. Turbomach. 128 (2006) 53. doi:10.1115/1.2098789.

Appendix

Appendix A: Determination of uncertainty in Frossling number

Uncertainty calculations were done using the method explained by Moffat [29]. Estimated uncertainties for various parameters such as the heat transfer coefficient, Nusselt number, Reynolds number and Frossling number were calculated in this study.

Estimated uncertainty for local Frossling number measured using IR camera:

The overall convective flux at any point on the cylinder measured using an IR camera is given by equation 2.

$$q''_{conv} = q''_{in} - q''_{rad} - q''_{cond,r} - q''_{cond,s}$$

Using equations 1, 3, 4 and 5 in equation 2, the following equation is obtained.

$$q''_{conv} = h_c(T - T_{inf}) = \frac{V^2}{RA} - \epsilon\sigma(T^4 - T_{inf}^4) - \frac{T - T_{inf}}{\pi D(R_{PVC} + R_{insulation})} + k_{Al}t_{Al}\frac{\partial^2 T}{\partial s^2}$$

The convection heat transfer coefficient can be found using equation 2 and 6.

$$h_c = \frac{V^2}{RA(T - T_{inf})} - \epsilon\sigma(T^2 + T_{inf}^2)(T + T_{inf}) - \frac{1}{\pi D(R_{PVC} + R_{insulation})} + \frac{k_{Al}t_{Al}}{(T - T_{inf})}\frac{\partial^2 T}{\partial s^2}$$

The uncertainty in h_c (Uh_c) can then be found as shown

$$C_1 = \frac{\partial h}{\partial V} = \frac{2V}{RA(T - T_{inf})}$$

$$C_2 = \frac{\partial h}{\partial T} = -\frac{V^2}{RA(T - T_{inf})^2} - \epsilon\sigma(3T^2 + 2TT_{inf} + T_{inf}^2) + \frac{q_{cond,s}}{(T - T_{inf})^2}$$

$$C_3 = \frac{\partial h}{\partial T_{inf}} = \frac{V^2}{RA(T - T_{inf})^2} - \epsilon\sigma(T^2 + 2TT_{inf} + 3T_{inf}^2) - \frac{q_{cond,s}}{(T - T_{inf})^2}$$

$$Uh_c = \sqrt{C_1^2 \delta V^2 + C_2^2 \delta T^2 + C_3^2 \delta T_{inf}^2}$$

The uncertainty in Nu (UNu) is given by

$$\frac{\partial Nu}{\partial h_c} = \frac{D}{k}$$

$$UNu = \frac{D}{k} Uh_c$$

The uncertainty in Frossling number can be found using Uh_c and UNu

$$\frac{\partial Fr}{\partial Nu} = \frac{1}{\sqrt{Re}}$$

$$\frac{\partial Fr}{\partial v} = -\frac{Fr}{2v}$$

The jet centerline velocity is calculated based on the readings obtained by a pitot tube connected to a differential manometer. The uncertainty in velocity can be found using the accuracy of the manometer. The centerline velocity is measured by the formula

$$v = \sqrt{2g\mathrm{h}}$$

Therefore the uncertainty in jet velocity (δv) is

$$\delta v = \frac{v}{2h} \delta h$$

The percentage uncertainty in Frossling number can be then found

$$UFr\% = \frac{UFr}{Fr} * 100$$

The uncertainty budget for the parameters measured are as tabulated below in table 3.

Table 3: Uncertainty budget for calculation of parameters

δV (Supplied Voltage)	0.01 V
δT (Surface Temperature)	0.2 ^{0}C
δT_{inf} (Ambient Temperature)	0.2 ^{0}C
δh (accuracy of manometer)	0.03 inches

For a jet Reynolds number of 43500 and a supply voltage of 61.5 V to the heater, the uncertainty in average Frossling number was found to be 4.4%.

Estimated uncertainty for local Frossling number measured using a heat flux sensor:

The overall convective flux at any point on the cylinder measured using an IR camera is given by the equation

$$q''_{conv} = h_c(T - T_{inf}) = \frac{V_s}{S} - \epsilon\sigma\left(\mathrm{T}^4 - T_{inf}^4\right)$$

$$h_c = \frac{V_s}{S\left(T - T_{inf}\right)} - \epsilon\sigma\left(\mathrm{T}^2 + T_{inf}^2\right)(T + T_{inf})$$

The uncertainty in h_c (Uh_c) can then be found as shown

$$C_1 = \frac{\partial h}{\partial V_s} = \frac{1}{S\left(T - T_{inf}\right)}$$

$$C_2 = \frac{\partial h}{\partial T} = -\frac{V_s}{S\left(T - T_{inf}\right)^2} - -\epsilon\sigma\left(3\mathrm{T}^2 + 2TT_{inf} + T_{inf}^2\right)$$

$$C_3 = \frac{\partial h}{\partial T_{inf}} = \frac{V_s}{S\left(T - T_{inf}\right)^2} - -\epsilon\sigma\left(\mathrm{T}^2 + 2TT_{inf} + 3T_{inf}^2\right)$$

$$Uh_c = \sqrt{C_1^2\delta V_s^2 + C_2^2\delta T^2 + C_3^2\delta T_{inf}^2}$$

The uncertainty in Nusselt number and Frossling number were calculated in a manner similar to the method used for estimated uncertainty of local Frossling number measured using IR camera. Uncertainty budget for measurement of V was taken as 0.000001V and the budget for the other uncertainties are as shown in

table 3. For a jet Reynolds number of 43500 and a supply voltage of 61.5 V to the heater, the uncertainty in average Frossling number was found to be 3.9%.

Appendix B: Method of estimation of convection heat transfer coefficient of a human forearm using an IR camera

An estimating of convective heat flux from a human forearm was done using an IR camera.

Experimental setup

Experiments on measuring the heat flux and temperatures of a normal clothed human body were conducted with the help of a Virginia Tech student. An IR camera was used to measure temperatures and calculate the heat flux. The measurements of different sections of the boy were taken with the student wearing black cotton clothes and standing in an upright posture. The emissivity of cotton fabric was obtained from previous studies to be 0.7[34]. The emissivity of the skin was taken to be 0.96.

Data Reduction analysis

The total heat transfer coefficient (h_t) was found using equation.

$$h_t = \frac{q_{met}}{\sum_i A_i(T_i - T_{inf})}$$

Where q_{met} is the metabolic rate of a human body, A_i is the surface area of the ith body part. T_i is the surface temperature of the ith body part. A reasonable value of metabolic rate for persons performing sedentary activities was obtained from previous studies [35–37] to be 1 Met (1 Met = 58.15 W/m^2). The convective heat transfer coefficient (h_c) from a particular body part, i can then be found using the equations.

$$q''_{conv} = h_t(T_i - T_{inf}) - q''_{rad}$$

$$h_c = \frac{q''_{conv}}{T - T_{inf}}$$

Results and discussion

Convective heat transfer coefficient from a human forearm was estimated based on the temperature readings using the IR camera. Figure 17 shows a sample image from the IR camera. Figure 18 shows the average

temperature measurements of different body parts using an IR camera. Area percentages for different body parts were obtained from previous studies [19,38]. Convective heat transfer coefficient for the forearm was estimated to be 4.4 $W/m^2/K$ based on a metabolic rate of 1 Met obtained from previous studies. This is slightly greater than the results obtained by R.J. De Dear et al. [18] (3.8 $W/m^2/K$) because clothing reduces the heat transfer, due to an increase in resistance and thus increases heat transfer in the exposed regions.

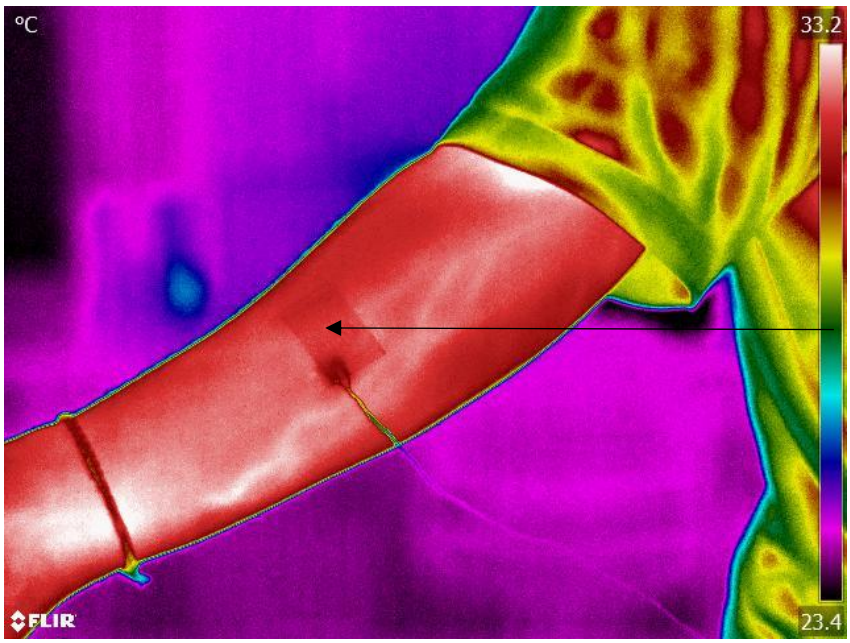

Figure 17: Measurement of temperature of human forearm using an IR camera

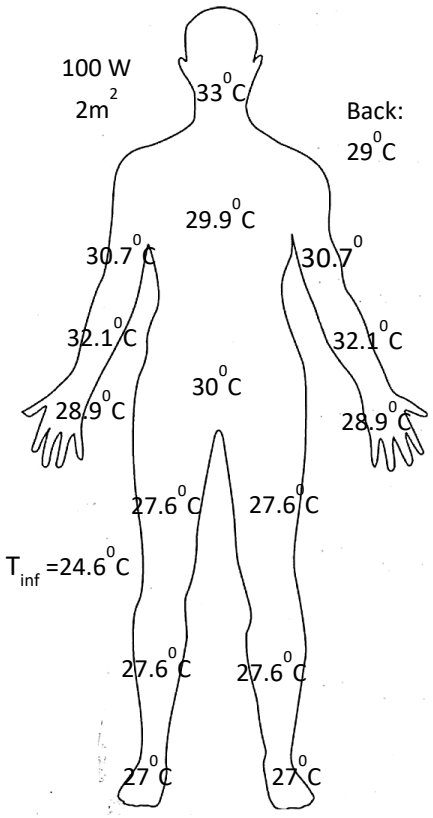

Figure 18: Temperature measurements of the human body obtained using an IR camera

Appendix C: Construction of a paper grid for measurement of angles using an IR camera

Colban et al.[39] used grid vortices from a 1 cm^2 square placed on the curved surface to perform a third-order polynomial surface transformation to take care of the curvature effect. For this study, a method similar to the one used by Balasubramanium et al. is used [12] to mark angular measurement on an IR camera feed. A 14 cm (5.5'') wide and 23 cm long sheet of paper was used to cut out 36 equal rectangular strips of width 3.2 mm and equally spaced apart by 3.2 mm. The calculation were done based on the circumference of the cylinder and that 5^0 along the curved surface of the cylinder would be (5x23/360) cm on a sheet of paper wrapping the cylinder. The strip cut in such a way that the end of the strip lines up with the middle of the cylinder when the top edge of the sheet is placed on one edge of the heater. The length of the cut was 7 cm to provide good visibility of the heated surface when viewed with an IR camera. A drawing of such a grid is as shown in figure 19.

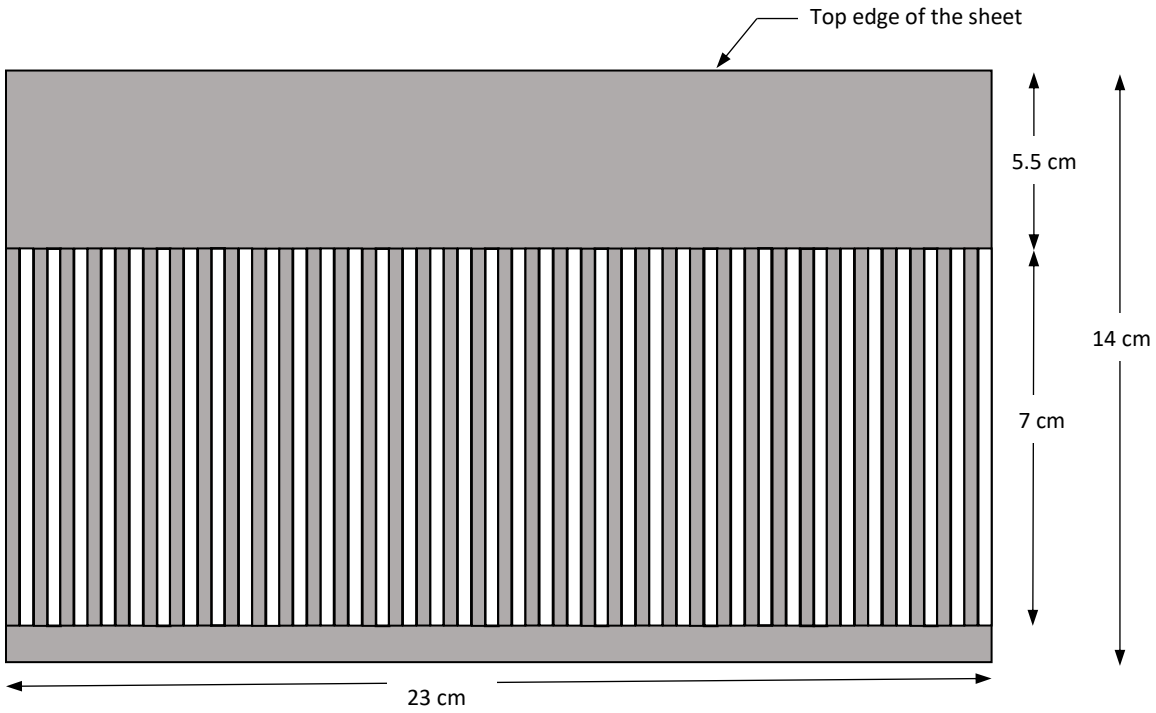

Figure 19: Grid used for angular measurements

The sheet is wrapped around the cylinder such that the 14 cm edges are parallel to the axis of the cylinder. Each of the cut and uncut strips form an alternating 5^0 measurement pattern.

Experimental procedure

The heater was first set to desired value of heat flux. The angle measurement grid was then wrapped around the cylinder. The IR camera was used to view the front portion or the back portion of the cylinder as shown in figure 20. The grid vortices can be seen using the IR camera because of differences in temperature readings between the alternating strips of the grid. These points were marked on the IR feed using FLIR tools. Successive markings on the IR image represents 5^0 increments in surface angle along the cylinder's circumference. The grid can then be taken off and the rest of the experimental procedure can be continued.

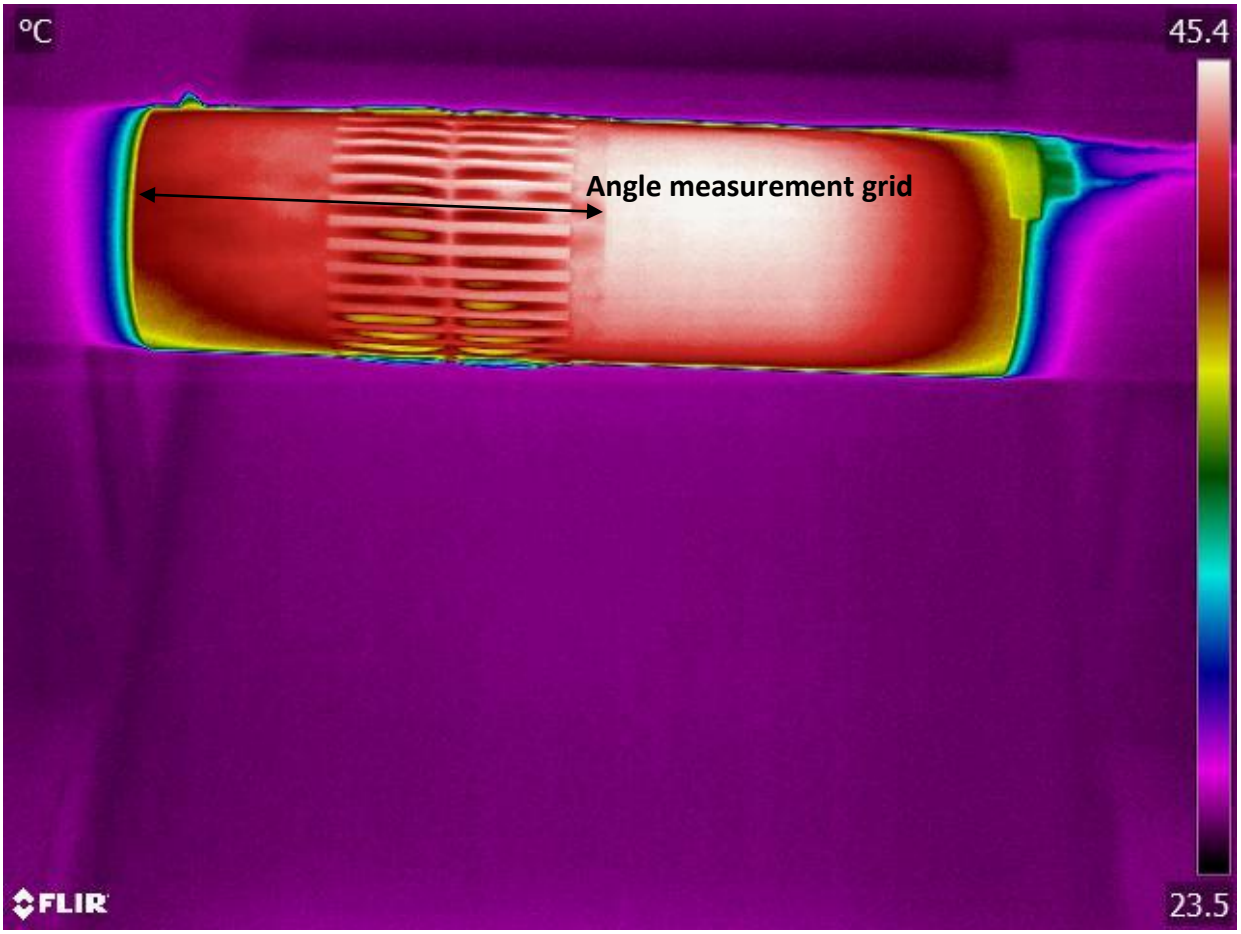

Figure 20: IR camera image of the grid wrapped around the heated cylinder

Appendix D: Quantification of limits of IR camera viewing angle to account for directional emissivity of curved surfaces

The angle between the surface normal and the normal to the camera has a significant effect on the accuracy of the IR camera reading. As mentioned earlier, this is caused due to the directional emissivity of surfaces. When a curved surface such as a cylinder, is viewed normally using an IR camera, parts of the curved surface of the cylinder that are curved away from the IR camera emit lesser IR radiation towards the camera. This, in turn, results in an inaccurate measurement of surface temperature. Previous studies have shown that for viewing angles greater 60^0, a measurement error of 0.4^0C was observed. Such errors can lead to high uncertainties in low temperature measurements. Therefore, proper quantification of limits of the

camera-viewing angle is necessary. A method similar to the one used by Balasubramanium et al.[12] was used for the quantification.

Experimental Setup

The cylinder used for jet impingement studies was heated using an AC power supply, providing a supply voltage of 60V for generating uniform heat flux across the heater. The cylinder is placed vertically to eliminate any changes in temperature due to natural convection along the circumference of the cylinder. The cylinder is viewed using an IR camera at a viewing angle perpendicular to the axis of the cylinder. The angle measurement grid is placed on the cylinder and the 5^0 angle markings are marked on the IR camera feed in FLIR tools. The grid is removed and the cylinder is allowed to reach steady state. The differences in temperature between the marked points are noted and the limits of the viewing angle are taken to be the angular displacement between the points on either side of the normal to the IR camera where there is a maximum temperature difference of 0.2^0C.

Results

Figure 21 shows the image of the heat cylinder viewed using the IR camera. The line shows the extent of the angular displacement where the temperature difference is less than 0.2^0C. The angular displacement was found to be 110^0, which is $\pm55^0$ on either side of the normal viewing angle of the IR camera. Therefore, for measurement of temperatures on the front face of the cylinder surface facing a jet, the IR camera's normal viewing angle is set at 45^0 from the stagnation point on the cylinder. Measurements are taken $\pm45^0$ on either side of the normal ($\theta = 0^0$ to 90^0). For the rear side of the cylinder, the IR camera is placed at 135^0 from the stagnation point and measurements of temperatures at angular displacement $\theta = 0^0$ to 90^0 are recorded.

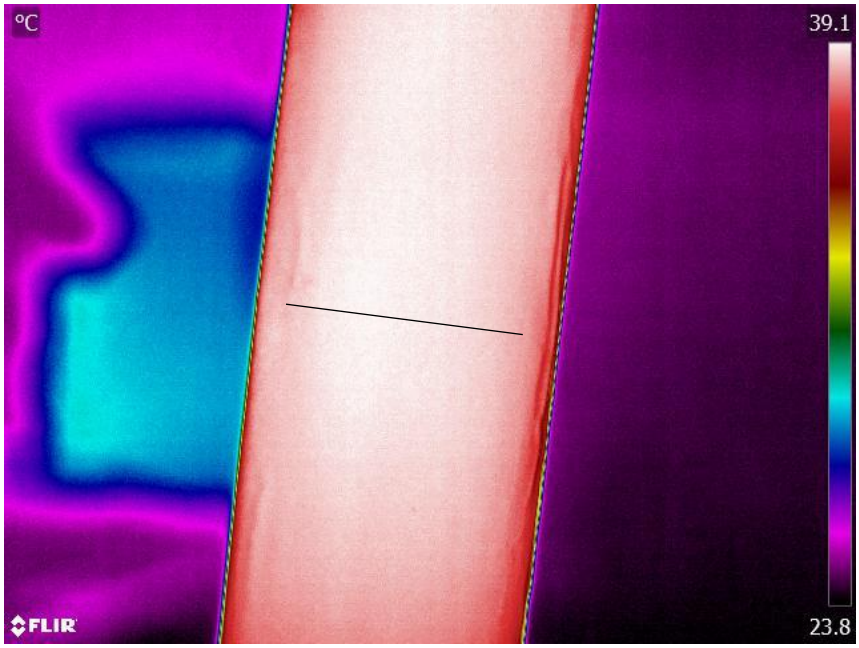

Figure 21: Effects of viewing angle on a cylindrical surface

Appendix E: Construction of control environment for natural convection experiments

Experiments on natural convection were conducted in both an open environment (open air-conditioned room) and under controlled environment. The controlled environment should be closed from external disturbances and should be large enough to accommodate the cylinder. Another important factor to be taken care of is the rate of heating of ambient air in the control environment due to heat transfer from the heated cylinder. For conducting controlled natural convection experiments, there should not be any significant heating of ambient air. The heat capacity of the air, C inside the control environment is given by

$$C = \rho V C_p$$

The power output from the cylinder or a forearm can be then calculated

$$P = q'' * A$$

The approximate temperature increase of ambient air inside the control environment can be obtained as follows

$$P = C\frac{dT}{dt} = C\frac{\Delta T}{\Delta t}$$

$$\Delta T = \frac{P}{C}\Delta t$$

Based on the above equations it was found that an enclosure of dimensions 48 cm x 48 cm x 36 cm gave a temperature rise of ~0.2^0C/minute when the heated cylinder is emitting a total heat flux of 75 W/m^2.

While conducting experiments, the heater on the cylinder was heated and allowed to reach steady state outside the enclosure. The cylinder was then placed inside the enclosure and data was recorded for a period of 1 minute. The cylinder was taken out and a table fan was used to cool the enclosure. The experiment is then repeated with the sensor at a different angle with respect to the horizontal level.

Appendix F: Heat transfer results from natural convection experiments in open and controlled environments

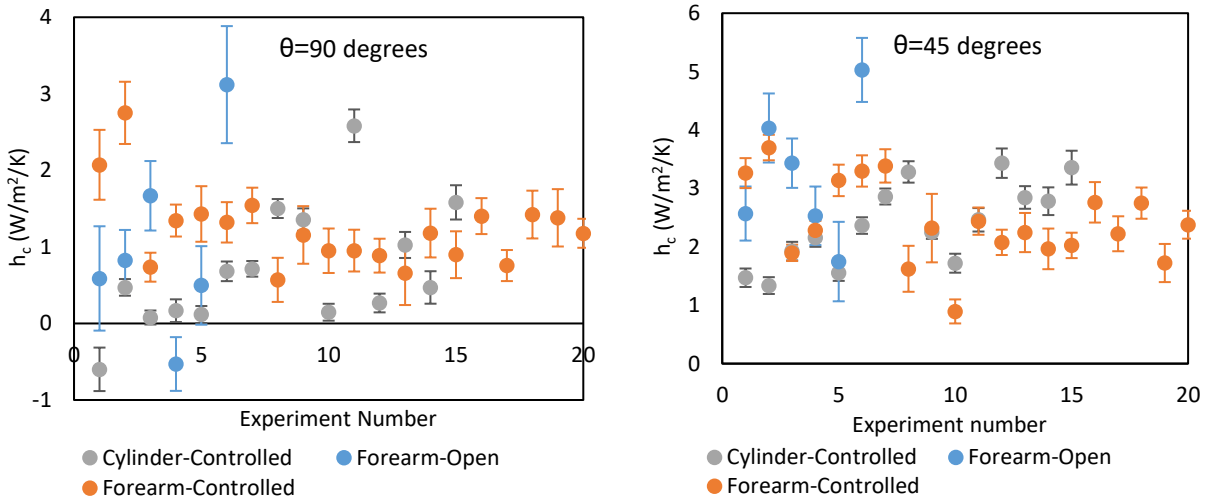

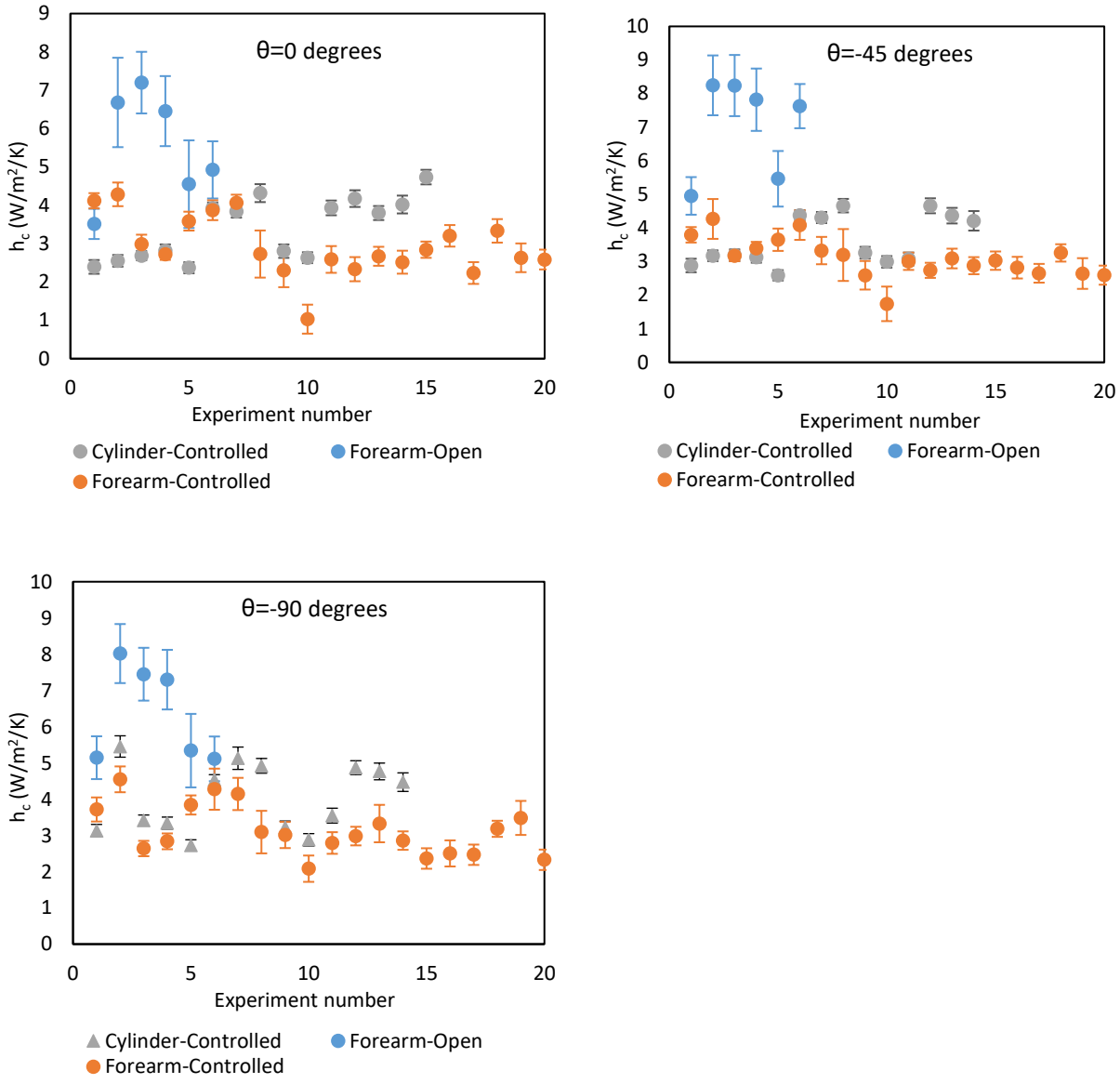

Figure 22: Convection heat transfer coefficient results from natural convection from cylinder and forearm in open and controlled environments for different angular positions on the circumference